Partitioning of Mg, Sr, Ba and U into a subaqueous calcite speleothem

Russell N. Drysdale[1,2], Giovanni Zanchetta[3], Ilaria Baneschi[4], Massimo Guidi[4], Ilaria Isola[5], Isabelle Couchoud[2,1], Leonardo Piccini[6], Alan Greig[7], Henri Wong[8], Jon D. Woodhead[7], Eleonora Regattieri[3], Ellen Corrick[1,2], Bence Paul[7], Christoph Spötl[9], Eleonor Denson[1], Jay Gordon[1], Stephane Jaillet[2], Florian Dux[7], John C. Hellstrom[7]

1. School of Geography, The University of Melbourne, 3010 Victoria, Australia
2. Laboratoire EDYTEM, UMR CNRS 5204, Université Savoie Mont Blanc, Université Grenoble Alpes, 73376 Le Bourget du Lac, France
3. Dipartimento di Scienze delle Terra, Universita degli Studi di Pisa, Pisa 56126 Italy
4. Istituto di Geoscienze e Georisorse IGG-CNR, via Moruzzi 1, 56126 Pisa, Italy
5. Istituto Nazionale di Geofisica e Vulcanologia, Sezione di Pisa, via della Faggiola 32, 56126 Pisa, Italy
6. Dipartimento di Scienze delle Terra, Universita degli Studi di Firenze, Via la Pira 4, 50121 Firenze, Italy
7. School of Earth Sciences, The University of Melbourne, 3010 Victoria, Australia
8. Australian Nuclear Science and Technology Organisation, Lucas Heights, NSW 2234, Australia
9. Institut für Geologie, Universität Innsbruck, A-6020 Innsbruck, Austria

ABSTRACT

The trace-element geochemistry of speleothems is becoming increasingly used for reconstructing palaeoclimate, with a particular emphasis on elements whose concentrations vary according to hydrological conditions at the cave site (e.g. Mg, Sr, Ba and U). An important step in interpreting trace-element abundances is understanding the underlying processes of their incorporation. This includes quantifying the fractionation between the solution and speleothem carbonate via partition coefficients (where the partitioning (D) of element X (D_X) is the molar ratio [X/Ca] in the calcite divided by the molar ratio [X/Ca] in the parent water) and evaluating the degree of spatial variability across time-constant speleothem layers. Previous studies of how these elements are incorporated into speleothems have focused primarily on stalagmites and their source waters in natural cave settings, or have used synthetic solutions under cave-analogue laboratory conditions to produce similar dripstones. However, dripstones are not the only speleothem types capable of yielding useful palaeoclimate information. In this study, we investigate the incorporation of Mg, Sr, Ba and U into a subaqueous calcite speleothem (CD3) growing in a natural cave pool in Italy. Pool-water measurements extending back 15 years reveal a remarkably stable geochemical environment owing to the deep cave setting, enabling the calculation of precise solution [X/Ca]. We determine the trace element variability of 'modern' subaqueous calcite from a drill core taken through CD3 to derive D_{Mg}, D_{Sr}, D_{Ba} and D_U then compare these with published cave, cave-analogue and seawater-analogue studies. The D_{Mg} for CD3 is anomalously high (0.042 ± 0.002) compared to previous estimates at similar temperatures (~8°C). The D_{Sr} (0.100 ± 0.007) is similar to previously reported values, but data from this study as well as those from Tremaine and Froelich (2013) and Day and Henderson (2013) suggest that [Na/Sr] might play an important role in Sr incorporation through the potential for Na to outcompete Sr for calcite non-lattice sites. D_{Ba} in CD3 (0.086 ± 0.008) is similar to values derived by Day and Henderson (2013) under cave-analogue conditions, whilst D_U (0.013 ± 0.002) is almost an order of magnitude lower, possibly due to the unusually slow speleothem growth rates (<1 μm a^{-1}), which could expose the crystal surfaces to leaching of uranyl carbonate. Finally, laser-ablation ICP-MS analysis of the upper 7 μm of CD3, regarded as 'modern' for the purposes of this study, reveals considerable heterogeneity, particularly for Sr, Ba and U, which is potentially indicative of compositional zoning. This reinforces the need to conduct 2D mapping and/or multiple laser passes to capture the range of time-equivalent elemental variations prior to palaeoclimate interpretation.

Keywords: trace-element geochemistry, speleothems, calcite, partition coefficients, caves, palaeoclimate

1. INTRODUCTION AND BACKGROUND

The trace-element geochemistry of calcium carbonate minerals is widely used to help reconstruct past environments across a wide range of time scales (Fairchild & Treble 2009). The mechanisms by which these elements are incorporated vary depending on the physical properties of the element (e.g. especially the charge and ionic radius – Bourdin et al. 2011), the carbonate mineral in question (usually either calcite or aragonite, e.g. Balboni et al. 2015; Wassenburg et al. 2016, Chen et al. 2016) and the mineralization environment (e.g. marine vs cave vs soil; Mucci & Morse 1983; Burton & Walter, 1991; Fairchild et al. 2000; Kelly et al. 2006). Key to understanding these mechanisms and interpreting trace-element variations in palaeoenvironmental archives is the quantification of the relationship between the trace element-to-calcium ratio [X/Ca] of the carbonate and that of the parent solution, known as the 'partition coefficient' [D_X]. This is defined empirically as:

$$D_X = \frac{[X/Ca]_{CaCO_3}}{[X/Ca]_{aq}} \quad (1)$$

Speleothems (e.g. stalagmites, flowstones) are palaeoclimate archives composed of calcium carbonate, usually in the form of the mineral calcite or aragonite (Fairchild & Baker 2012). They are formed from carbonate-rich waters that have permeated through limestone or dolomite host rock. When the waters reach an air-filled chamber with a lower partial pressure of carbon dioxide (PCO_2), CO_2 outgassing causes the solution to become supersaturated with respect to calcite (or aragonite) to a point where mineral precipitation occurs in the form of stalagmites, flowstones and other speleothem types.

In the last two decades, speleothems have emerged as valuable palaeoenvironmental archives because their source waters encode geochemical information on climate-driven shifts in rainfall, temperature and/or vegetation above the cave (Fairchild & Baker 2012). Their utility is further enhanced by the ability to date them accurately and precisely using U-Th and U-Pb methods (Cheng et al. 2009, 2016; Woodhead et al., 2006), which allows the assembly of high-quality palaeoclimate proxy time series.

The most widely used environmental proxies in speleothem studies are stable oxygen and carbon isotope ratios (expressed as $\delta^{18}O$ and $\delta^{13}C$, respectively) (Fairchild & Baker 2012). Changes in speleothem $\delta^{18}O$ are a function of the temperature of mineralisation in the cave and

drip-water $\delta^{18}O$ (Hendy & Wilson 1968; Schwarcz et al. 1976), with the latter generally regarded as the main driving factor (McDermott 2004; Lachniet 2009). Mean drip-water $\delta^{18}O$ values principally reflect the amount-weighted average of $\delta^{18}O$ of effective recharge at a cave site, which can be affected by seasonal changes in local hydrology (e.g. Markowska et al. 2016). The climate mechanisms controlling local rainfall $\delta^{18}O$ reflect a complex series of fractionation processes that take place between the original moisture source and the cave site (Lachniet 2009). Interpreting trends in speleothem $\delta^{18}O$ in terms of changes in, for example, rainfall amount, dominant air-mass trajectories and seasonality, can be challenging. The interpretation of speleothem $\delta^{13}C$ is similarly complex (Lauritzen & Lundberg 1999; McDermott 2004), particularly in determining the relative importance of climate-driven processes in the soil/epikarst and those occurring within the cave chamber (which may or may not be climate-driven) (Fairchild & Baker 2012). Thus, complementary sources of proxy information from alternative speleothem properties are useful for refining palaeoclimate reconstructions.

Trace-element geochemistry has emerged as the principal means by which to extract such complementary information (Johnson et al. 2006; Fairchild & Treble 2009; Griffiths et al. 2010; Fairchild & Baker 2012; Fohlmeister et al. 2012; Hartmann et al. 2013; Orland et al. 2014). Trace elements are sourced from aerosols, soils, vegetation, bedrock and/or sediment infills, and reach the growing speleothem as colloids, solutes or particulates (Fairchild & Treble 2009). Although a wide variety of elements has been investigated (Borsato et al. 2007; Zhou et al. 2008; Fairchild & Baker 2012; Day & Henderson 2013), most attention has been directed at elements that substitute for the calcium ion (Ca^{2+}) in the crystal structure, notably Mg^{2+}, Sr^{2+} and Ba^{2+} (Mucci & Morse 1983; Paquette & Reeder 1995; Rimstidt et al. 1998). Such elements are often sensitive to climate-driven changes in cave hydrology (Fairchild & Treble 2009; Day & Henderson 2013; Tremaine et al. 2013), and thus have considerable value in refining or reinforcing interpretations of stable isotope changes (Treble et al. 2005; Drysdale et al. 2006; Cruz et al. 2007; Liu et al. 2013; Wong et al. 2015; Ünal-Imer et al. 2016; Bernal et al. 2016). This can be further complemented by data from other isotope systems (e.g. Ca and U isotopes – Owen et al. 2016; Hellstrom & McCulloch 2000; Drysdale et al. 2005).

A number of previous studies have determined partition coefficients directly using natural cave waters and speleothems (Gascoyne 1983; Fairchild et al. 2001; Tremaine & Froelich 2013; Wassenburg et al. 2016) and through laboratory 'cave-analogue' experiments (Huang &

Fairchild 2001; Day & Henderson 2013), but their number is few owing to the practical difficulties of farming calcite in caves and mimicking the intricate physico-chemistry of caves in a laboratory setting. The great majority of the research conducted to date has been aimed largely at partitioning between drip-waters and stalagmites (or analogues thereof), whereas partitioning into other speleothem types remains largely unexplored.

In this study we investigate the partitioning of trace elements into subaqueous speleothem calcite. Subaqueous speleothems have rarely been considered in palaeoenvironmental research. Most speleothem studies to date have been based on either stalagmites or flowstones, which usually yield higher-resolution records. However, the partitioning of trace elements into these stalagmites or flowstones is likely to differ from that of subaqueous speleothems because of the strong contrast in physico-chemical conditions, which govern reaction kinetics and, by implication, trace-element partitioning (Fairchild & Baker 2012). Whilst subaqueous speleothems have been shown to be potentially susceptible to radiometric dating problems (Edwards et al. 1993; Moseley et al. 2016), their great value lies in their ability to capture long, continuous palaeoclimate records (Winograd et al. 1992; Drysdale et al. 2012). Being mostly fed by multiple, rather than single, points of vadose percolation flux, pool-water geochemistry is likely to be more representative of a regional response to environmental change than stalagmites because, provided the pool is large enough, it potentially integrates recharge from a larger surface above the cave and is less susceptible to the nuances of an individual drip-water flow path. Here we present results from a series of near-monthly water chemistry measurements from an Italian cave pool conducted over the period from May 2009 to March 2012. We assess the temporal patterns of hydrochemical changes in the pool and compare with the observed rainfall for the same period, then combine the pool-water and subaqueous calcite [X/Ca] to calculate a series of partition coefficients (D_{Mg}, D_{Sr}, D_{Ba} and D_{U}). We then compare these new data with published partition coefficients from mostly cave and cave-analogue studies.

2. STUDY SITE AND SAMPLING

The water and calcite samples used in this study were collected from Antro del Corchia, a large cave system developed in Mesozoic dolomites, marbles and dolomitic marbles of the Alpi Apuane of western-central Italy (Piccini et al. 2008; Baneschi et al. 2011) **(Fig. 1)**. The samples come from a cave pool ('Laghetto Basso') **(Fig. 2 & 3)** that has developed on the floor of a large, well-decorated chamber called the Galleria delle Stalattiti (GdS). The chamber is situated ~400 m vertically below the surface at ~835 m above sea level, and is located about 1 km from

the nearest natural entrance to the cave (Piccini et al., 2008). The microclimate is relatively stable, typical of deep-cave environments: based on continuous monitoring between 2002 and 2006, the mean (±1 s.d.) temperature, wind speed and relative humidity of the chamber is 8.4 (0.3) ˚C, 0.09 (0.07) m s^{-1}, and 100.0 (0.2) %, respectively (Piccini et al. 2008). Rainfall reaching the cave is derived primarily from air masses moving eastwards from the North Atlantic (Drysdale et al. 2004). The Alpi Apuane massif presents a topographic barrier to these air masses, and the orographic rainfall it promotes produces an annual average of over 3000 mm at the watershed near Monte Corchia (Piccini et al. 2008).

The rock sequence above the GdS has been subjected to multiple phases of metamorphism (Carmignani & Kligfield 1990; Kligfield et al. 1986). The Paleozoic basement, consisting mainly of phyllites (Filladi Inferiori), porphyritic meta-volcanics (Porfiroidi e Scisti Porfirici), quartzites (Filladi Superiori) and local lenses of graphitic schist and meta-dolostone (Dolomie a Orthoceras), is overlain by the dolomitic 'Grezzoni', which is the basal portion of the metamorphosed Apuane carbonates (**Fig. 2; Table A1**) (Carmignani & Giglia 1984; Conti et al. 1993). The Grezzoni has been overfolded such that the basement sits topographically above the carbonates and is exposed at the surface directly above the GdS chamber. However, whilst percolation waters almost certainly enter the karst along the basement-dolomite contact, surface hydrography precludes significant karst recharge via direct surface runoff from the basement itself **(Fig. 2)**.

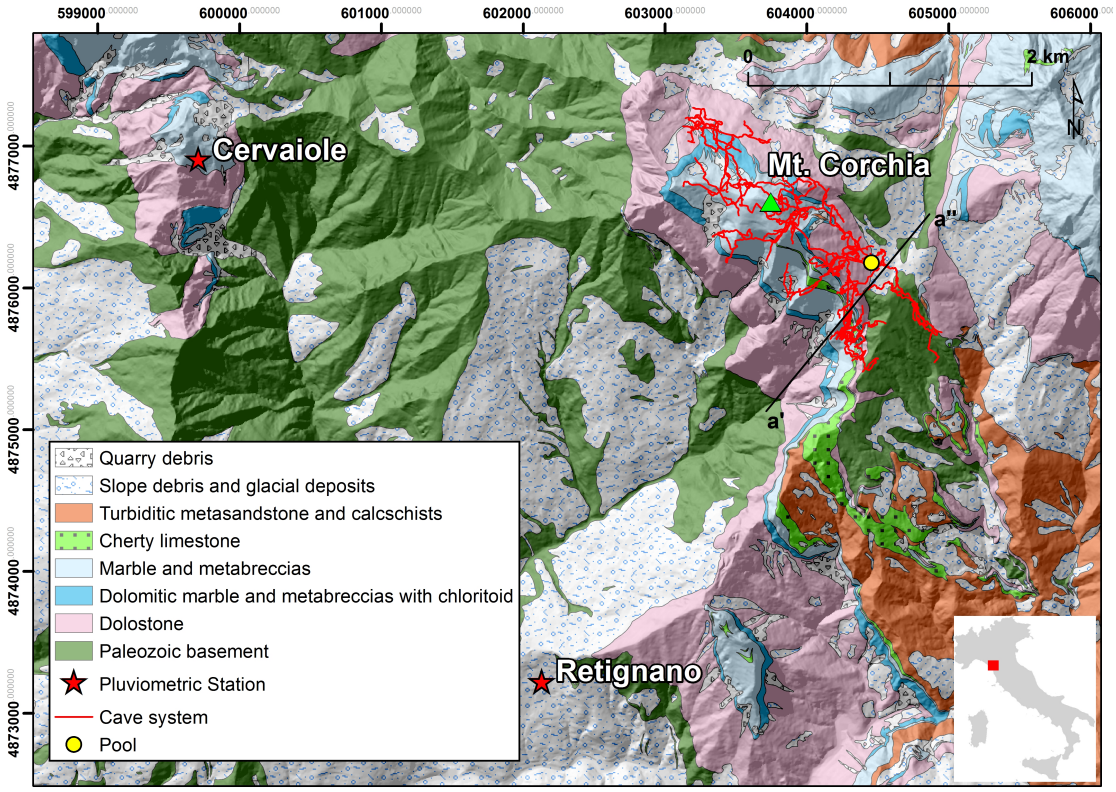

Figure 1: Location and geology of the study area. A geological cross section between a' and a" is shown in Figure 2c.

Based on a preliminary cave survey conducted in May 2017, the minimum volume of Laghetto Basso has been calculated at 15.2 m^3, 80% of which is contained within a single basin **(Fig. 3)**. This basin is fed largely by a drapery of stalactites that have grown from percolation waters issuing from fractures aligned parallel to the strike of the carbonate beds that form the chamber's ceiling. It drains across a narrow sill at the southern end (Drysdale et al. 2012). Drip-water discharge monitoring at nearby site CNR2, conducted over a two-year period starting in October 2007, suggests relatively constant dripping rates (varying by less than ~50% around a mean value of 89 drips per hour: Baneschi et al. 2011), suggesting some degree of dampening of seasonal recharge variations due to the long flow path and volume of vadose storage. One-off instantaneous drip measurements conducted in May 2017 showed that the pool receives at least ~37 L/day, equivalent to a mean residence time of the pool waters of almost one year. Based on the CNR2 drip-rate data, the month of May is a good proxy for mean annual drip rate (mean value: 93 drips per hour; May 2008 and 2009 mean value: 95 drips per hour), suggesting the instantaneous pool measurements offer a reasonable first-order estimate of turnover rate. Stable isotope data show that the pool waters are isotopically very stable (Piccini et al. 2008; Baneschi et al. 2011; Daëron et al. 2019), suggesting the percolation waters are well mixed by the time they arrive in the pool.

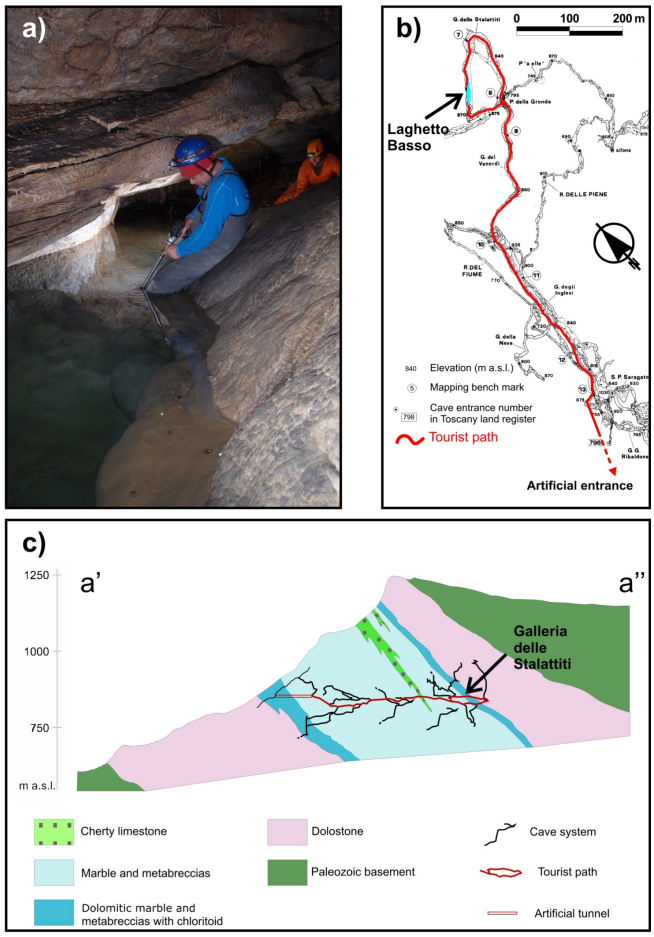

Figure 2: (a) Laghetto Basso pool, from where the CD3 core was drilled. (b) Plan-view map of the part of Corchia Cave where this study was carried out. Galleria delle Stalattiti is located in the far north. (c) Topographic and geological cross section through Monte Corchia along a traverse (shown in Figure 1) incorporating the Galleria delle Stalattiti.

The wetted perimeter of Laghetto Basso is coated with a continuous crust of "mammillary calcite" of variable thickness, similar to the well-known subaqueous vein calcite of Devils Hole, Nevada (e.g. Winograd et al., 1992; Kolesar and Riggs, 2004). The crust morphology varies according to that of the underlying bedrock floor, which is, in parts, littered with broken speleothems. In the largest basin of Laghetto Basso, several ~hemispheric domes occur, from one (CD3) of which the core sample (CD3-12) for this study was drilled **(Fig. 2)**.

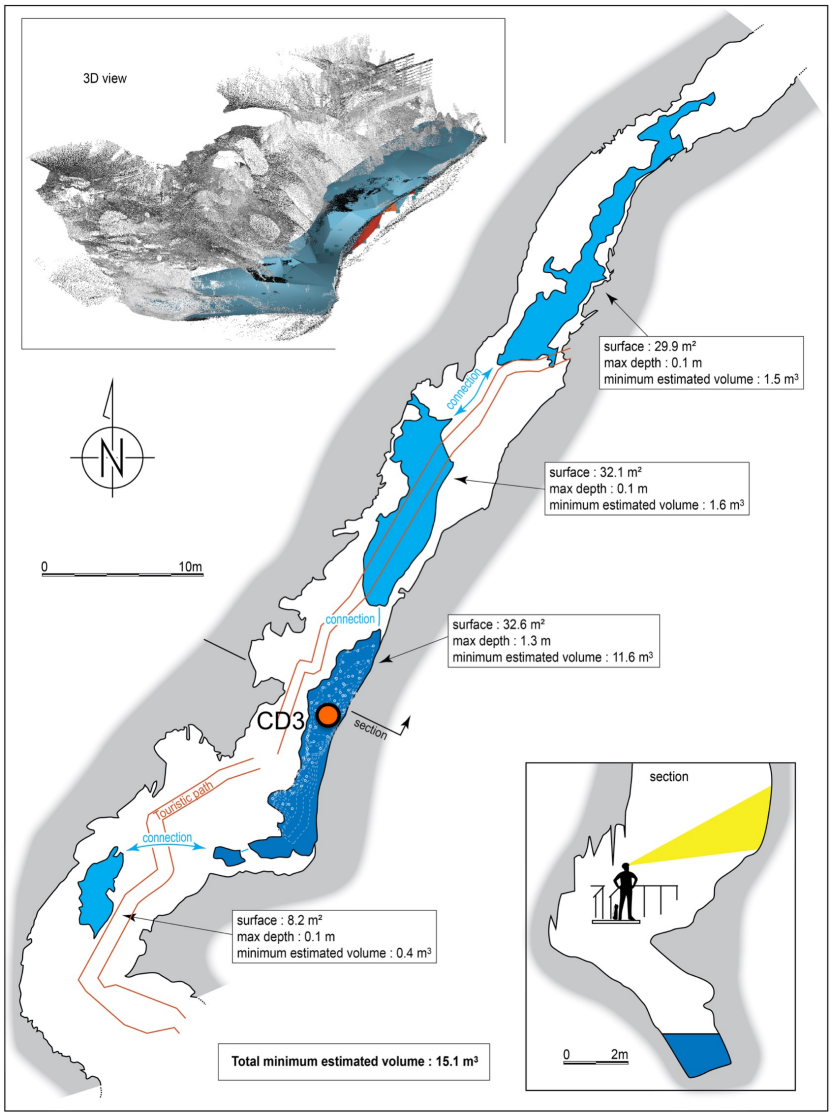

Figure 3: Plan and section view of Laghetto Basso derived from a 3D cave survey conducted in May 2017. Volumetric data are shown for the individual basins. The basin hosting the subaqueous speleothem CD3 is the largest.

3. METHODS

3.1 Water sampling and analysis

Water temperature, electrical conductivity (EC) and pH were measured directly in the Laghetto Basso water using a portable multi-parameter meter (Delta OHM Instruments). Accuracy is 0.5% for conductivity, 0.25% for temperature and 0.1 for pH. The pH and EC sensors were calibrated prior to each sampling trip with certified standard buffer solutions (pH 4 and 7 solutions, and 147, 717.5 and 1413 µS cm^{-1} solutions).

Total alkalinity was measured in the field within 1-2 hours of sampling by HCl (0.1 N) titration according to Gran's method (Gran 1952) using methyl-orange as the indicator solution. The

error of the analysis is 0.01 meq L^{-1}. Additional samples were stored in chemically inert polyethylene bottles with a screw cap and a separate internal closure plug for additional air-tight sealing. One aliquot of each was filtered through a 0.45-μm cellulose-acetate syringe filter then split into two acid-washed/MQ water-rinsed bottles: the first was acidified with suprapur HNO_3 (2% v/v, TraceSELECT Fluka, with U, Ba, Sr < 0.5 μg/kg) for U, Sr and Ba analysis, whilst the second fraction, reserved for cation Ca and Mg analysis, was acidified with HCl (2% v/v, Sigma-Aldrich puriss. p.a. with Ca < 0.5 and Mg< 0.1 mg/kg) in order to prevent any post-sampling calcite precipitation. A second unacidified aliquot was analysed for anions and Na. A "blank" sample (MQ-water filtered and acidified in the field) was prepared to check for contamination during sampling. All solutions were kept refrigerated at 4 °C until analysis.

Major cations (Ca, Mg and Na) were analysed by atomic absorption spectrometry (Perkin-Elmer model 3110), and anions by ion chromatography (Dionex-100). The minor elements Sr and Ba were measured by inductively coupled plasma atomic emission spectrometry (ICP-AES, Perkin-Elmer Optima 200DV) at the Institute of Geoscience and Earth Resources, Consiglio Nazionale delle Ricerche (CNR), Pisa, Italy. Uranium analysis was carried out using inductively coupled plasma mass spectrometry (ICP-MS Perkin Elmer model ELAN 5000) at the EUROLAB laboratories in Nichelino, Italy.

The analytical reproducibility (±) for Ca, Mg, Na, K, Cl and SO_4 was ≤2%, and ≤5% for Sr, Ba, and U. The detection limit for Ba and Sr was 1 ppb and for U was 0.5 ppb; these elements were analysed on undiluted subsamples. All analyses included replicates, blanks and quality-control standards measured with every set of unknown samples, the concentrations of which were calculated from daily calibration curves. The calcite saturation indices (defined as the log of the quotient of ionic activity product and solubility product) and the partial pressure of CO_2 in equilibrium with the solution, expressed as $\log PCO_2$, were determined from the measured drip-water chemistry using SOLVEQ (Reed 1982).

3.2 Speleothem sampling

Modern samples were obtained from the outer surface of drill core CD3-12, which was recovered from CD3, a ~30-cm-high subaqueous dome-shaped mound, in December 2012 using a battery-powered drill fitted with a 45-mm-internal-diameter, diamond-crowned core barrel (Spötl and Mattey 2012). The core measures 260 mm in length and was drilled to bedrock. It was cut longitudinally into two halves which were then polished. The speleothem bears no

visible signs of alteration and, like other cores drilled from the same pool (Drysdale et al., 2012), comprises a compact crystalline calcite fabric of a predominantly columnar-fascicular optic type (*sensu* Neuser & Richter 2007; Frisia 2015), with large polycrystals up to several centimetres long (length-to-width ratio commonly > 10:1), oriented roughly perpendicular to the growth surface, and characterised by undulatory extinction (in cross-polarized light). This fabric is common to speleothems with a relatively high Mg content (typically from 10,000 to 30,000 ppm). In stalagmites and flowstones, this has been shown to most likely develop where source-water Mg/Ca lies between ~0.4 and ~3 mol/mol and where the calcite saturation index (SI_c) is between ~0.3 and ~0.5 (Frisia 2015).

Each half of CD3-12 was ultrasonically cleaned in double-deionised water to remove any loose particles that might be present on the active growth surface. It was then clamped face down to the edge of a bolting plate fitted to the moving stage of a milling lathe (**Fig. A1**). Fifteen surface carbonate samples (7 from one half, 8 from the other, giving a total of 15 aliquots) were then carefully abraded individually from discrete ca. 1 cm^2 regions of the active outer growth surface using a Dremel hand tool fitted with a 0.4-mm diameter diamond bur with the assistance of a 3x magnification lense. A single pass across each crystal was made, and, using the bur diameter as a guide, the depth of abrasion was conservatively estimated to be no more than 100 μm. The carbonate was collected on weighing paper suspended on a scissor jack positioned beneath the speleothem tip (**Fig. A1**). After sampling over each region, the core section was unclamped, and the remaining powder transferred to the weighing paper by tapping the section. The yield was placed into a clean 1.5 mL microcentrifuge tube. Prior to sampling the next region, the section was cleaned using compressed air.

The yield from each region was split into several fractions for a range of analyses (including clumped isotopes: Daëron et al. 2019). Two aliquots of ~0.2 – 1.0 mg were set aside for trace element analyses by ICP-MS in two different laboratories: the Isotope Geochemistry Laboratory at the School of Earth Sciences, The University of Melbourne (herein 'UM'), and the Elemental Laboratory, Isotope Tracing in Natural Systems, the Australian Nuclear Science and Technology Organisation (herein 'ANSTO').

3.3 Speleothem age

Exploratory uranium-series dating of CD3 suggested a basal age of around 1 Ma (Drysdale et al. 2008). This has been confirmed by comparing stable isotope profiles from Corchia Cave

stalagmites dated by U-Pb, including stalagmite CC8 reported in Bajo et al. (2012), with isotope profiles from the base of CD3 (our unpublished data). Ages reported in Drysdale et al. (2012) from core CD3-1 (drilled in 2007; length: 260 mm), covering the depth range of ~40 to ~50 mm from the top, span 229±5 to 295±8 ka, consistent with a basal age of the order of 1 Ma. Verifying a 'modern' age at the top of CD3, on the other hand, has proved somewhat more challenging. U-Th measurements on powders carefully scraped from the very outer surface give ages up to several thousand years before present, suggesting growth had stopped well before the monitoring period for this study. However, a subsequent chronology **(Table A2)** used to anchor CD3 $\delta^{18}O$ and $\delta^{13}C$ time series reveals that stable isotope patterns are up to several thousand years older than those from a well-dated coeval stalagmite (CC26) (Zanchetta et al. 2007; Bajo et al. 2016; see supplementary information in **Appendix 1** and **Fig. A2 to A6**). This indicates that CD3 yields older-than-true ages, and that the pool water is susceptible to the same dating issue recently proposed for Devils Hole (Nevada, USA): the growing surface of subaqueous calcite scavenges excess ^{230}Th produced by decay of ^{234}U in the water column (Edwards & Gallup 1993; Moseley et al. 2016). To place CD3 onto an accurate age scale and to quantify the age offset, we synchronised its $\delta^{18}O$ and $\delta^{13}C$ profiles to those of CC26 (**Fig. A5**). The results show that the mean offset over the Holocene is ~2 kyr. The $\delta^{18}O$ and $\delta^{13}C$ at the top of CD3 (Daëron et al. 2019) is consistent with the $\delta^{18}O$ and $\delta^{13}C$ composition of the tips of stalagmites actively growing within a 20 m radius of the pool (**Fig. A5**). Therefore, whilst we cannot definitively demonstrate that CD3 is active today due to its slow growth rate and the incorrect U-Th dates, the combined evidence of: (i) the corrected CD3 age profile; (ii) the excellent agreement between the isotopic composition of the CD3 outer surface and that of actively growing stalagmites near the pool; and (iii) the fact that the speleothem has grown continuously over almost the last million years, including glacial periods (Drysdale et al. 2012), would indicate that the speleothem is actively growing today. We also note that the slow growth rate precludes the detection of the radiocarbon bomb pulse, as has been possible for faster-growing speleothems (Genty & Massault 1997; Mattey et al. 2008; Hodge et al. 2011; Griffiths et al. 2012).

Based on the thickness of its Holocene section (~4 mm; **Fig. A6**), and the likelihood of relatively stable growth rates based on previously studied Holocene stalagmites from Corchia (Zanchetta et al. 2007; Bajo et al. 2016; Isola et al. 2019), the sampled surface calcite of CD3-12 conservatively integrates the last ~300 yr of growth.

3.4 Calcite analyses

3.4.1 Solution analyses of CD3-12 core-top calcite

For solution analyses at UM, the calcite aliquots were dissolved in 1 mL of 5% twice-distilled HNO_3 containing a nominal 2 ppb of internal standards (^{6}Li, ^{84}Sr, ^{235}U and In). The vial contents were mixed by shaking then dispensed into tubes for analysis. A further 1 mL was added to the now-empty vials and the process repeated to ensure all solutes were removed. For the purpose of preparing standards, data from previous laser-ablation ICP-MS analyses on Laghetto Basso calcite enabled the matrix of the speleothem to be matched as closely as possible. A 50:50 mix of a previously analysed speleothem solution and a basalt rock standard solution were used for calibration for a better matrix match than the pure silicate rock standards normally used for calibration. Samples were run on an Agilent 7700x ICP-MS. The calibration standard was run every 8 samples to correct for external drift after internal standard normalisation.

At ANSTO, the aliquots were digested in 3% Merck suprapur HNO_3 which was spiked with an internal standard to a final concentration of 20 ppb. Standards were prepared using the same spiked 3% HNO_3 solution. The standard concentrations were prepared according to previously determined approximate sample concentrations. The elements were analysed using a Varian 820MS ICP-MS with internal standards used to correct for matrix effects and instrument drift. Standard checks were analysed after every 20th sample.

In both laboratories, elements were normalized to ^{43}Ca and molar ratios calculated. The reproducibility for the calibration standard ratios at UM were 1.2% for (^{25}Mg:^{43}Ca), 1.0% for (^{88}Sr:^{43}Ca), 1.0% for (^{137}Ba:^{43}Ca), and 0.9% for (^{238}U:^{43}Ca), whilst at ANSTO they were 1.6% for (^{25}Mg:^{43}Ca), 1.6% for (^{88}Sr:^{43}Ca), 1.2% for (^{137}Ba:^{43}Ca), and 1.3% for (^{238}U:^{43}Ca).

3.4.2 Laser-ablation analyses of the outermost layer of CD3-12 calcite

To complement the calcite solution ICP-MS analyses, we used laser-ablation inductively coupled plasma mass spectrometry (LA-ICP-MS) to investigate the level of homogeneity of Mg, Sr, Ba and U concentrations in the outermost layer of CD3-12 (**Fig. A7**). To achieve this, analyses were conducted on a polished section of CD3-12 using a 193-nm Ar-F excimer laser-ablation system coupled to an Agilent 7700x quadrupole ICP-MS. The laser targetted the outermost 7 μm, running parallel to the growth surface. The operating conditions of the laser and ICP-MS, as well as the elements/masses that were analysed, are summarised in **Table 1**.

The sample was first ultra-sonically cleaned in double-deionised water for 15 minutes then fitted into the sample holder of the laser system, which moves in *x, y* via a computerised stage. The RESOlution laser-ablation system, fitted with a Laurin Technic two-volume ablation cell, is driven by *GeoStar* software (Resonetics) and was set up to ablate seven traverses of unequal length along the outermost 7 μm (e.g. Woodhead et al., 2007) (**Fig. A7**) and using a 7-μm-square ablation profile. Based on a mean Holocene growth rate of ~0.34 μm yr^{-1} (Appendix 1), this is likely to integrate the last ~21 years of growth up to the date of core drilling (December 2012), encompassing the period over which the water sampling was conducted. Although the accuracy and precision of the calcite LA-ICP-MS results are unlikely to compete with those from the solution analyses due to the lack of a compatible matrix-matched standard against which to calibrate raw laser data, the advantage lies in its outstanding spatial detail. The technique should resolve significant changes in element concentrations that might be related to, for example, the mode of element incorporation (e.g. replacement, interstitial) or crystal zoning (Reeder & Grams 1987).

Each ablation 'spot' (n=120 in total) was ablated for 15 s at a pulse rate of 5 Hz and a fluence of 5 J cm^{-2}. The spacing between successive ablation centres was 8 μm. Ablation took place in an environment of ultra-high-purity helium, with the ablated aerosol carried into the mass spectrometer under an ultra-high-purity argon stream. Elemental concentrations were calibrated against the NIST SRM610 glass reference standard (measured three times during the session) with ^{43}Ca used as an internal standard to monitor and correct for instrument drift. Raw mass spectrometry data were reduced using *Iolite* software (Hellstrom et al., 2008; Paton et al., 2011). A laser log file produced by *GeoStar* records the laser state and the position of the laser spot against a timestamp. For each spot, the first 2 s were cropped to eliminate residual surface contaminants after ultrasonication, whilst the last 8 s were cropped due to down-hole diminution of yield and mass fractionation. This resulted in a final data acquisition time of ~5 s per spot, equivalent to 24 or 25 data points per spot. The mean analytical uncertainty on the four elements based on the internal 95% standard error (2 s.e.) on the three NIST610 glass standard measurements is between 3.0 and 3.8%.

Finally, the mean and standard deviation from the LA-ICP-MS Mg, Sr, Ba and U data were calculated and combined with the pool water [X/Ca] to derive a comparison series of D_X values.

3.5 Rainfall data

To determine the sensitivity of pool-water trace element concentrations to cave recharge, hourly pluviometric data from the nearest rain gauging stations (Cervaiole: ~4.5 km WNW of Monte Corchia, elevation 1140 m a.s.l.) and Retignano (~3 km SSW of the cave entrance, 440 m a.sl.) **(Fig. 1 & 2)** were aggregated to produce monthly series over the period of water sampling.

4. RESULTS

4.1 Pool-water chemistry

The pool-water chemistry of Laghetto Basso is summarised in **Table 2**; additional data, including charge balances, saturation indices and PCO_2 values, are contained in **Table A3**. The Laghetto Basso water temperature is stable at 7.9 ± 0.4˚C (2σ), which is to be expected from a deep-interior chamber. The pH of the waters is slightly alkaline, and for most of the sampling period only fluctuated within a narrow envelope (± 0.2 units). The ion chemistry indicates that the waters are of low ionic strength for a karstic environment (Drysdale 2001; McDonald et al. 2007; Tremaine & Froelich 2013). The Mg^{2+} concentrations are relatively high, and yield [Mg/Ca] persistently above 1 (mean ± 1 s.d. 1.18 ± 0.06). The mean concentrations of Sr (56.0 ± 3.5 μg L^{-1}) and Ba (23.8 ± 2.1 μg L^{-1}) produce [Sr/Ca] and [Ba/Ca] (0.88 ± 0.11 mmol mol^{-1} and 0.24 ± 0.04 mmol mol^{-1}) that are significantly (~3x) enriched compared to the Grezzoni dolomite bedrock [Sr/Ca] and [Ba/Ca] values (0.29 mmol mol^{-1} and 0.07 mmol mol^{-1} respectively (Azzaro et al. 1987; Cortecci et al 1999; **Table A1**). Sulphate is also present at moderate concentrations (up to ~32 mg L^{-1}: **Table A3**). Pool-water PCO_2 averages around twice that of the open atmosphere, whilst mean calcite saturation is ~0.27 ± 0.18 (2σ).

The concentration of each ion is relatively invariant, with coefficients of variation (CVs, based on 2σ) less than 10% for all species; the CVs of the major elements Ca^{2+}, Mg^{2+} and HCO_3^- are less than 4% (**Table 2**). A consequence of the ~invariant ion concentrations is stable [X/Ca], with mean and 2σ uncertainties for [Mg/Ca], [Sr/Ca], [Ba/Ca] and [U/Ca] being 1.175±0.055 (mol/mol), 0.879±0.058 (mmol/mol), 0.238±0.021 (mmol/mol) and 0.039±0.010 (μmol/mol) respectively (**Table 2**). Such invariant solution chemistry and the availability of naturally accreted subaqueous calcite indicates that Laghetto Basso is ideally suited for yielding well-constrained calcite partition coefficients.

4.2 Temporal patterns in pool-water chemistry and rainfall

Plots of the major hydrochemistry parameters and the derived indices (PCO_2 and the calcite saturation index, SI_c) against time are shown in **Fig. 4**. On first inspection, there does not appear to be any patterns that would indicate clear, and mutually consistent, hydrologically driven changes over the monitoring period **(Fig. 4)**. Prominent peaks occur simultaneously in Sr^{2+} and Ba^{2+} between July and August 2009; U concentrations rise around the same time but the peak persists well after Sr^{2+} and Ba^{2+} fall, and the peaks are not consistently matched by other ions through the same period. On the other hand, the decrease in Mg^{2+} shortly after (October 2009) is to some extent expressed in both Ca^{2+} and HCO_3^-, suggesting a dilution effect, but not in pH, PCO_2 or SI_c. If a dilution effect were responsible this should also impact Sr and Ba, but both of these ions are ~invariant through this interval. Overall, there is a suggestion of a weak downward trend in HCO_3^- and Ca^{2+} (if one ignores the last data point). Both Ba^{2+} and, particularly, U show a downward trend from late 2011; Sr^{2+} also shows a steady decrease from late 2011. These latter changes are proportionally greater than the subtle overall decreases in HCO_3^- and Ca^{2+}. The pH also tends to decrease through time but correlations with the downward trending ions are weak and statistically insignificant.

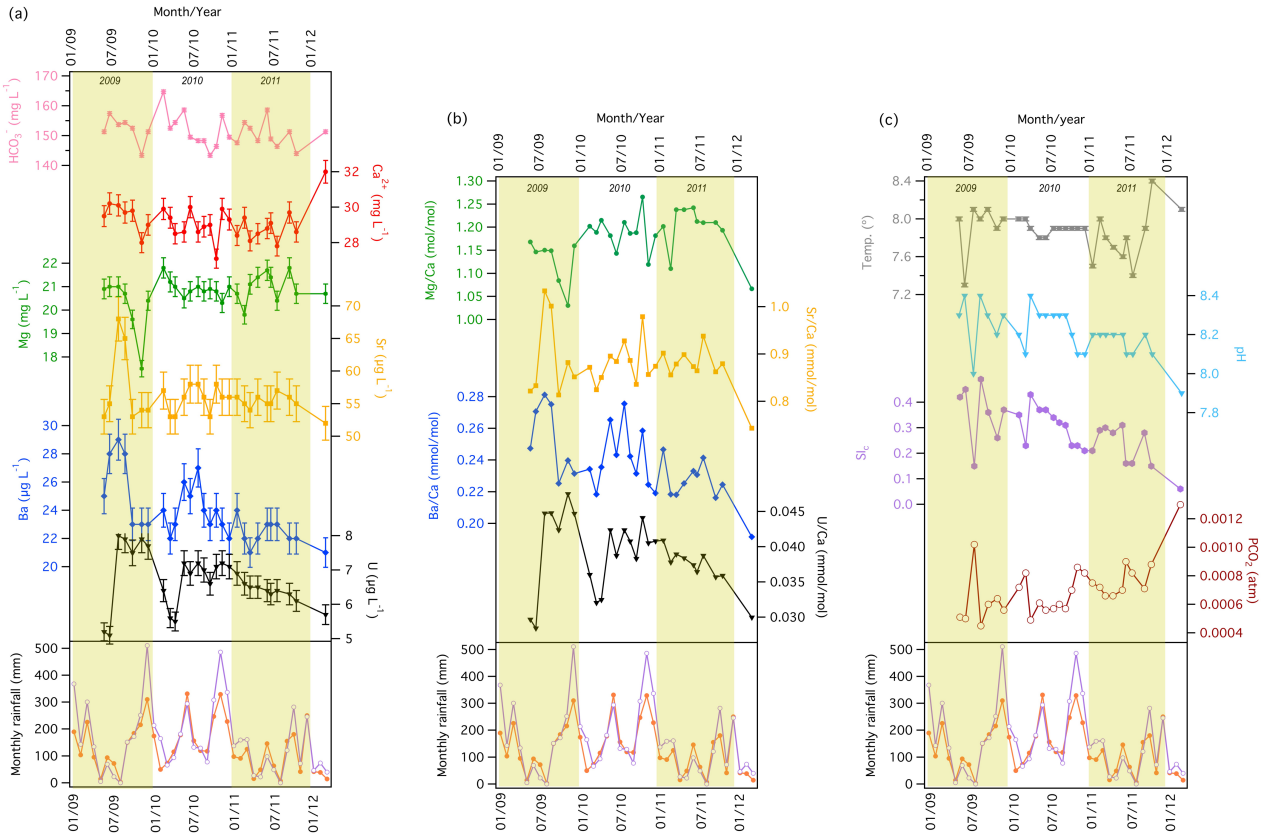

Figure 4: Comparison of Laghetto Basso pool-water geochemistry and local rainfall amount through the monitoring period: (a) ion concentrations; (b) ion ratios; and (c) temperature, pH, PCO_2 and SI_c. Each lower panel shows the monthly rainfall amounts for two nearby rainfall gauging stations Cervaiole (1140 m a.s.l., orange) and Retignano (440 m a.s.l., purple). Vertical errors bars in panel (a) are 1 s.d. analytical uncertainties.

The monthly rainfall patterns for Cervaiole and Retignano (**Fig. 4**) over the monitoring period broadly follow one another. Peaks occur in autumn to mid winter in all years, although conditions were wetter for 2009-10 and 2010-11 than in 2011-12, and the spring-to-early-summer peak in 2010 is significantly higher than the corresponding periods for the years either side.

4.3 Calcite geochemistry

4.3.1 Solution ICP-MS data from calcite surface scrapings

The [X/Ca] ratios from the surface calcite of CD3-12 are shown in **Table 3**. The mean values from both UM and ANSTO laboratories compare favourably within their respective 2σ uncertainties, although there are some systematic offsets that imply analytical incongruencies between the two sets of analyses. The mean [Mg/Ca] and [Ba/Ca] measured at UM are 1.3% and 7.3% higher than those measured at ANSTO, respectively, whilst the mean [Sr/Ca] is 2.2% lower.

The degree of scatter in molar ratios amongst the 15 calcite samples is relatively small for [Mg/Ca], [Sr/Ca] and [Ba/Ca], with CVs (based on 2σ) ≤3.3% **(Table 3)**; variability in [U/Ca], however, is more than twice that for the other ratios.

4.3.2 LA-ICP-MS analysis of calcite from the outermost ~7 μm

Table 4 and **Fig. 5** summarise the results of the LA-ICP-MS analyses of the outer rim of CD3-12; the raw data from each spot along each of the seven traverses are shown in **Table A4**. The data from each 5-s spot measurement yields a mean and 95% standard error for each of the four elements. These standard errors provide an approximation of the analytical precision of the spot analysis, assuming there is no significant downhole change in element concentrations, which is reasonable because the 7 μm × 7 μm laser profile reaches a depth of only ~2.5 μm across the period of ablation. The average standard error for each element based on the standard errors of all 120 spots provides an estimate of the overall analytical uncertainty of the sample measurements. The standard deviation from the mean values of all 120 spots for each element, on the other hand, indicates the variability in each element's concentration across the outermost 7 μm of CD3-12, and thus provides a measure by which to compare the variability in concentrations from the calcite solution ICP-MS data in section 4.3.1.

The overall variability in the laser data is higher than that for the solution data **(Table 4)**, which is to be expected given the higher resolution of the laser spot compared to the area (~ 1 cm^2) and thickness (not exceeding 100 μm) of the calcite sampled from the core top for the solution ICP-MS analyses. The range of concentrations of each element measured by LA-ICP-MS is also well in excess of the variability observed in the three NIST610 analyses (range 5.3% to 6.6%, 2 s.e.) conducted before, during and after sample acquisition. Thus, the laser analyses appear to capture real variability, both within and between most traverses. For example, all elements show variability along traverses 2 and 6, whilst the variability across traverse 3 is minimal. Furthermore, the rank order of variability for each element is similar in both analyses, with Mg having the least variability and U having the greatest.

4.4 Partition coefficients

Partition coefficients (D_X) were derived by combining the UM and ANSTO CD3-12 solution trace element datasets. We first applied the reduced χ-squared test (Reiners et al. 2017) to determine if the UM and ANSTO calcite measurements for each element were drawn from the same population. The calculated χ-squared statistic, or mean square weighted deviation (MSWD), is below the critical value of χ for each of the paired [X/Ca] means at the 95% probability level, indicating that each pair is drawn from the same population. Accordingly, error-weighted means were calculated for each ratio along with their error-weighted 95% uncertainties (bottom panel of **Table 3**). Applying equation (1) and combining the calcite and pool water [X/Ca] fractional uncertainties in quadrature yields the mean ± 1σ partition coefficients for Mg, Sr, Ba and U shown in **Table 5.** Partition coefficients are also shown for CD3-12 derived from the pool-water [X/Ca] and laser-ablation [X/Ca] data from the outermost ~7 μm, with fractional uncertainties calculated in the same way. The two sets of partition coefficients for CD3 are statistically indistinguishable, although the uncertainty for the laser-derived measurements is larger.

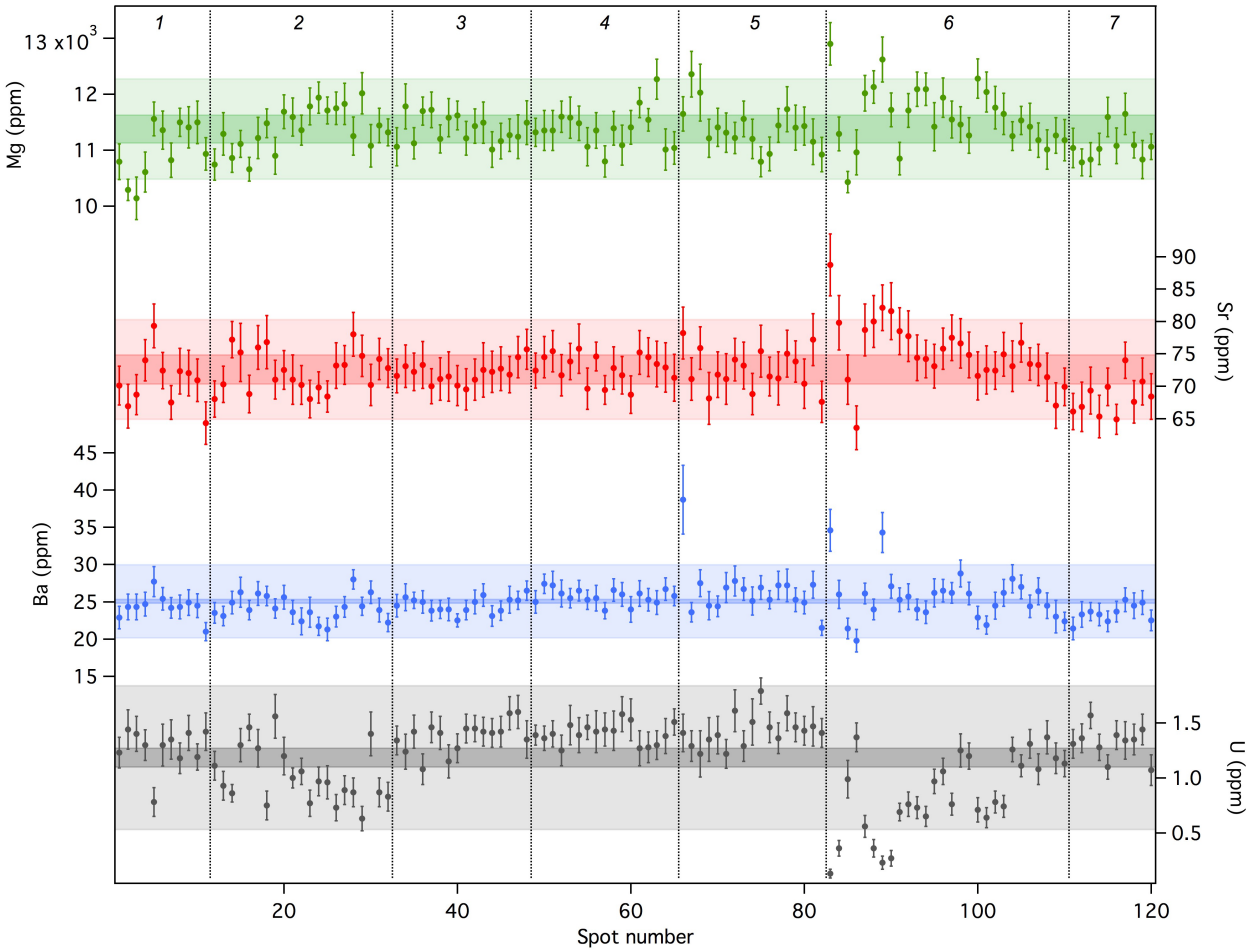

Figure 5: LA-ICP-MS trace element results (Mg, Sr, Ba and U) based on seven discrete traverses (total number of spots: 120) along the outermost 7 µm of core CD3-12. Each data point represents the mean concentration based on a five-second analysis window; the individual error bars are the 2 s.e. of measurement. The vertical lines separate the individual traverses (numbered at the top; see Fig. A7 for the position of the traverse on the sample section). The lighter-coloured bands are 2 s.d. envelopes around the mean of all laser spot values, as quoted in bold in the lower panel of Table 4. To compare the variability between laser and solution data, the dark-coloured bands are the corresponding 2 s.d. envelopes for the averaged calcite solution-analysis results. These were derived by converting molar ratios to elemental concentrations using the data in Table 3, and applying a Ca concentration of 39% (considering CD3 Mg concentrations of ~1%). The dark-coloured bands were then centred on the LA-ICP-MS average for each element.

5. DISCUSSION

5.1 Low ionic strength waters of Laghetto Basso

The Laghetto Basso pool waters are of low ionic strength, with concentrations of major ions (Ca^{2+}, Mg^{2+} and HCO_3^-) being at the lower end of the spectrum of cave percolation waters. Part of the reason for this is the likelihood of low PCO_2 of the infiltrating waters as they enter the karst, which can be attributed to the low soil cover above the cave (Drysdale et al. 2004). Much of the surface above Corchia Cave is steep and devoid of substantive soil cover. Here, the ground is criss-crossed by fractures, which facilitates infiltration. This exposed, high-purity

carbonate rock produces negligible soil-forming insoluble residue. Instead, soils are confined either to lower-angle, largely debris-mantled slopes to the northeast and comprise almost entirely organic matter, or to solution features etched into the karst rock. The areas of greatest soil development above the cave occur on the phyllite basement rock, which crops out on the eastern flank of Monte Corchia and is vertically above the GdS. However, hydrographic constraints suggest that significant runoff from the basement is unlikely to reach this part of the karst (**Fig. 2**). The low ionic strength and low calcite saturation values of the pool waters (**Table A3**), and the subaqueous setting, are also undoubted contributors to the excessively slow growth rates of CD3-12 (Drysdale et al. 2012). The slow growth rates could also be influenced by the presence of relatively high [Mg/Ca] and SO_4^{2-} concentrations, which are known inhibitors of calcite crystal growth (Busenberg & Plummer 1989; Nielsen et al. 2016).

The most distinguishing feature of the pool hydrochemistry, however, is its overall stability through time when compared to cave waters reported in other studies (e.g. Fairchild et al. 2000; McDonald, et al. 2004; Tremaine & Froelich 2013; Casteel & Banner 2015), including those where measurements of pool waters have been made (Huang et al. 2001). This supports earlier assertions of hydrochemical stability of Laghetto Basso (Piccini et al. 2008) based on lower-frequency sampling between 1997 and 2006 (see summary in the lower panel of **Table 2**). This attests to the very deep-seated position of Laghetto Basso within the cave system and its dampening effect on hydrochemical variability.

The persistently high [Mg/Ca] in the pool waters (**Table 2**) exceeds the ratio predicted from the dissolution of the Grezzoni dolomite bedrock (Azzaro et al. 1987; Cortecci et al. 1999), suggesting that prior calcite precipitation (PCP) (Fairchild et al. 2000; Bajo et al. (2017) and/or incongruent dissolution of dolomite (Busenberg & Plummer 1982) are important processes controlling the evolution of the percolation waters upstream of the pool. PCP occurs when calcite is precipitated along the percolation-water flow path before it reaches the speleothem under study. This causes a loss of Ca^{2+} from solution and an increase in the [X/Ca] of the percolation water. The operation of each of these processes can be tested using correlation. If PCP were important, Ca would decrease as [Mg/Ca] increases (Fairchild et al. 2000), whereas incongruent dissolution of dolomite, a theoretically plausible process under the partially closed-system conditions that occur at Corchia (Bajo et al. 2017), should produce a positive correlation between Mg and [Mg/Ca] because Ca is consumed by $CaCO_3$ precipitation as further Mg is released by continued dissolution of dolomite according to the reaction:

$$CaMg(CO_3)_2 + 2H_2O + 2CO_2 \rightarrow Ca^{2+} + Mg^{2+} + 4HCO_3^- \rightarrow CaCO_3 + Mg^{2+} + 2HCO_3^- + CO_2 + H_2O \quad (2)$$

and owing to the lower solubility of dolomite. On the other hand, PCP should not increase Mg concentrations. For Ca vs [Mg/Ca] and Mg vs [Mg/Ca], both correlation coefficients are statistically significant ($p < 0.05$; $df = 26$; one-tailed Pearson r), but the correlation for Mg vs [Mg/Ca] is much higher (Panels a-b, **Fig. 6**). The pattern is the same for [Sr/Ca] and [U/Ca]: both pairs of r values are statistically significant, but Sr vs [Sr/Ca] and U vs [U/Ca] (panels c-d and g-h, **Fig. 6**) are much higher. For [Ba/Ca], the correlation with Ca is almost zero, whilst the correlation with Ba is 0.94 (panels e-f, **Fig. 6**). As noted earlier, however, [Sr/Ca] and [Ba/Ca] are ~3x enriched in the pool waters compared to the Grezzoni bedrock (Azzaro et al. 1987; Cortecci et al 1999; **Table A1**), whereas [Mg/Ca] are only ~1.2x enriched. Both [Sr/Ca] and [Ba/Ca] are also significantly correlated (Pearson's r correlation, $r = 0.71$, $df = 26$; $p < 0.05$; **Fig. 7)**, suggesting enrichment from a common source. If incongruent dissolution of dolomite were also contributing to enriched [Sr/Ca] and [Ba/Ca] we would expect both these ratios to be positively correlated with [Mg/Ca], but this is not the case **(Fig. 7)**. Instead, the enriched [Sr/Ca] and [Ba/Ca] may be sourced where a component of the infiltration waters exploits the contact between the Paleozoic basement rock and the Grezzoni. This may explain the matching peaks in mid 2009 and decreasing trends from mid 2011 in both Sr^{2+} and Ba^{2+}. The tendency for U to share some of the patterns of Sr^{2+} and Ba^{2+} suggests it is also partly derived from a non-dolomitic source such as the basement rock.

The pool water contains moderate concentrations of SO_4^{2-}, which is likely sourced from pyrite that is present throughout the Apuane metamorphosed carbonates (including the Grezzoni dolomite). An alternative source is anhydrite, which, according to Azzaro et al. (1987), is present in the Grezzoni sequence. However, this appears unlikely as it would also contribute more Ca^{2+} to the waters, and there is no excess Ca^{2+} in the pool-water chemistry. Weathering of pyrite can lead to sulphuric-acid dissolution of the carbonate host rock, and in a previous study (Bajo et al. 2017) from GdS mass-balance calculations indicate that such sulphuric-acid dissolution makes up one-third of the total dissolved carbonate content of waters, with the remainder derived from carbonic-acid dissolution involving soil CO_2. Therefore, whilst the observed Ca^{2+}-Mg^{2+}-HCO_3^- concentrations are lower than is usually found in karst systems,

they would be even lower were it not for a contribution from bedrock dissolution caused by sulphide weathering.

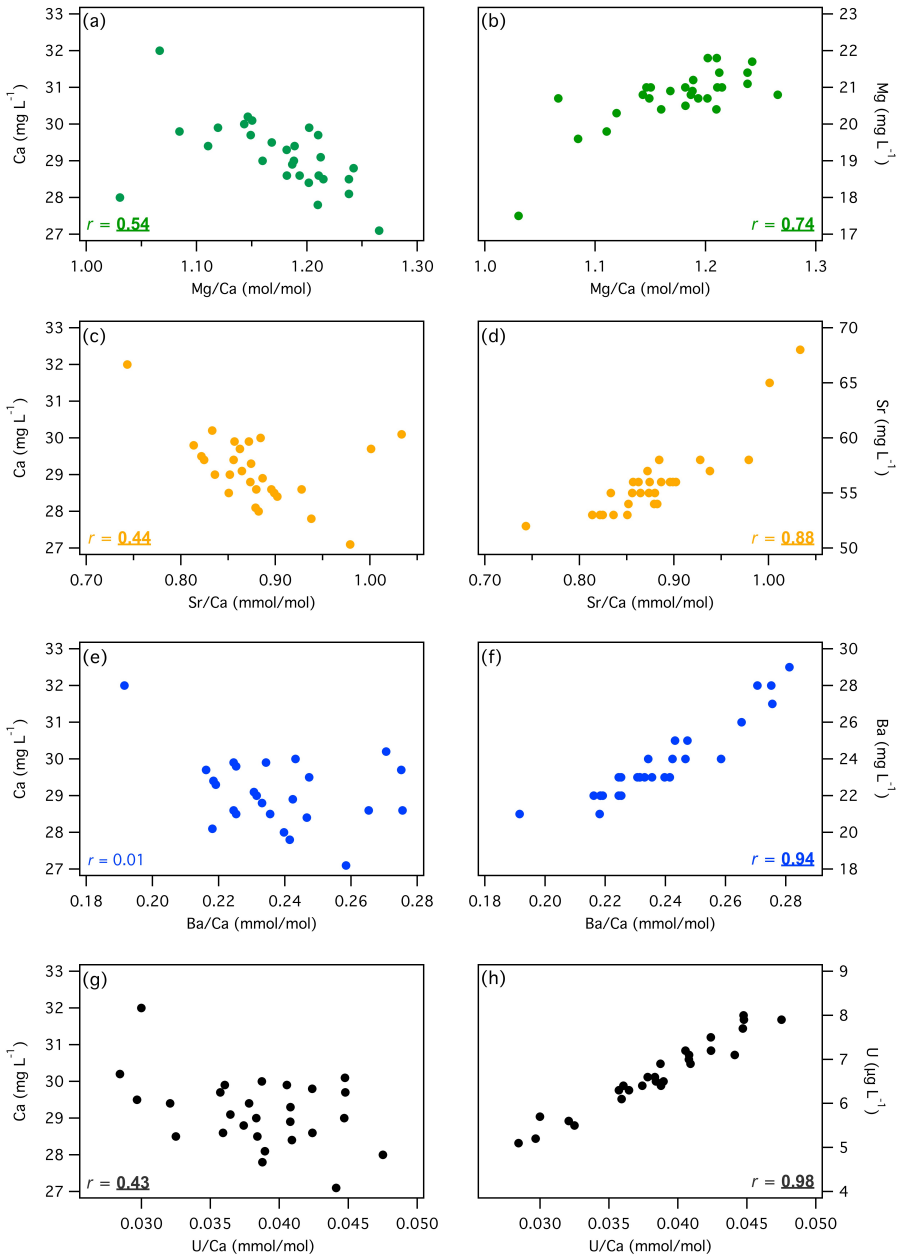

Figure 6: Scatterplots between aqueous [X/Ca] and their constituent ions for Laghetto Basso pool water. (a) Ca vs [Mg/Ca]; (b) Mg vs [Mg/Ca]; (c) Ca vs [Sr/Ca]; (d) Sr vs [Sr/Ca]; (e) Ca vs [Ba/Ca]; (f) Ba vs [Ba/Ca]; (g) Ca vs [U/Ca]; (h) U vs [U/Ca]. Pearson r correlation coefficients are shown (underlined values are statistically significant at $p \leq 0.05$).

5.2 Relationship between pool hydrochemistry and rainfall

The major hydrochemical parameters from Laghetto Basso show no clear and consistent relationships with rainfall through the sampling period **(Fig. 4)** when compared with monthly rainfall data from Cervaiole and Retignano over the same period. We tested this by interpolating

the rainfall series to the calendar dates of water sample collection and calculating Pearson *r* correlation coefficients between each ion and both rainfall series using lags between zero and 19 months (after which n < 10). Most *r* values are below 0.1 and only one significant correlation emerges: U vs Cervaiole rainfall (r = -0.64, df = 10, $p < 0.05$) with a lag of 18 months. This complacency is to be expected given the deep position of the cavern within the karst, and contrasts with many published case studies (e.g. McDonald et al. 2004; Mattey et al. 2008; Treble et al. 2013; Tremaine & Froelich 2013), though not all (Mattey et al. 2010; McDonald et al. 2007), where overlying rock thickness is sufficiently thin or permeable to record the effects of seasonal or event-based recharge variations on trace element concentrations.

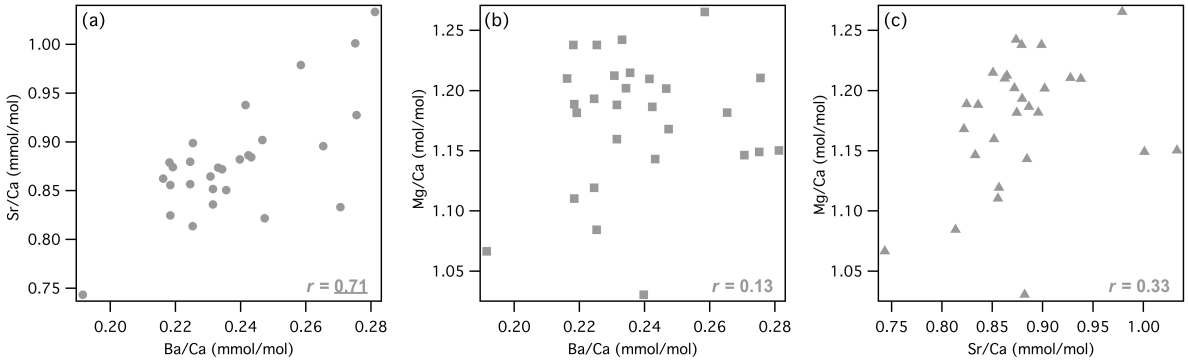

Figure 7: Scatterplots and Pearson *r* correlation coefficients of: (a) [Ba/Ca] vs [Sr/Ca]; (b) [Ba/Ca] vs [Mg/Ca]; and (c) [Sr/Ca] vs [Mg/Ca] from Laghetto Basso pool waters. The underlined *r* value is statistically significant at $p < 0.05$.

5.3 Trace element variations in 'modern' CD3 calcite

There is a degree of heterogeneous incorporation of trace elements into CD3-12 apparent from both solution analysis of large (1 cm^2) surface scrapings and, in particular, the higher spatial-resolution (49 μm^2) laser-spot analysis. Correlation coefficients for bivariate plots of the ANSTO and UM solution-analysis results reveal statistically significant *r* values for [Mg/Ca], [Sr/Ca] and [U/Ca] ($p < 0.05$, two-tailed Pearson *r* correlation test) **(Fig. 8)**. This indicates measurable inter-sample differences in these ratios (see the row of per cent values in **Table 3**) even at such a coarse spatial resolution, pointing to a degree of trace-element variability across the growing crystal surfaces. Paired sets of solution results for [Ba/Ca], on the other hand, reveal no correlation **(Fig. 6)**.

Both solution and laser datasets show consistent patterns in the degree of relative scatter around mean values, with Mg, Sr and Ba having the lowest scatter, and U having the highest scatter.

However, the magnitude of scatter is greater – up to eight times for U – in the laser data. The detection and nature of such scatter is important because of the growing use of microanalytical techniques for measuring trace elements in speleothems (Fairchild & Baker 2012), which raises the issue of how representative of the average time-equivalent trace-element concentrations in speleothem calcite are the concentrations determined from one or even a few individual laser scan lines. This has implications for deriving meaningful quantitative or semi-quantitative palaeohydrological information from elemental ratios.

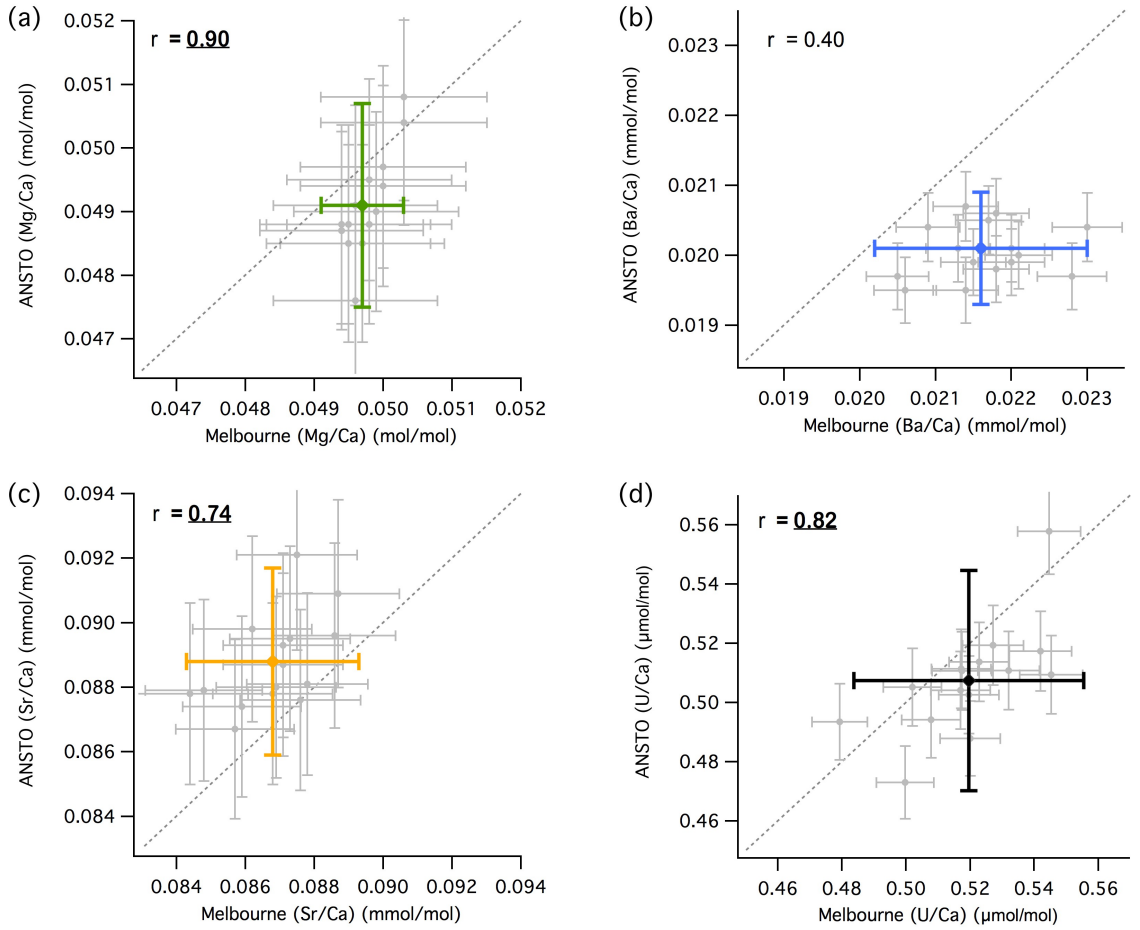

Figure 8: Scatterplots of individual Melbourne and ANSTO ICP-MS results for the CD3-12 calcite trace element ratios [Mg/Ca], 10^3*[Sr/Ca], 10^3*[Ba/Ca], and 10^6*[U/Ca] (grey points), along with mean values (coloured points). All error bars are 2 s.d. uncertainties. The diagonal dashed line represents parity ($y = x$) between the two sets of analyses. Pearson r values are shown, with underlined values being statistically significant at $p \leq 0.05$ ($df = 13$, two-tailed test).

The notion of heterogenous incorporation of trace elements into time-equivalent regions of calcite is well-documented in both laboratory and natural settings (Fairchild & Baker 2012) and is referred to as compositional zoning. It can occur between different crystal sectors with non-equivalent faces (intersectoral zoning) (Reeder & Grams 1987; Reeder & Paquette 1990) or

within the same crystal sector (intrasectoral zoning) (Paquette & Reeder 1995). In the case of the former, interfacial, time-equivalent trace-element concentrations can vary by up to a factor of eight, and are attributed to variable growth rates on different sectors or to the different surface structures characterising the non-equivalent faces (Reeder & Paquette 1990). Intrasectoral zoning occurs within a given single sector and is caused by anisotropic layer growth, giving rise to step-selective affinities for foreign ions that culminate in differential elemental partitioning (Paquette & Reeder 1990). As with intersectoral zoning, it is related to the fundamental structural properties of the crystal surface, and it co-exists with sectoral zoning (although the converse is not the case) (Paquette & Reeder 1995).

The traverse patterns evident in **Fig. 5** show some degree of covarying behaviour between pairs of elements. Scatterplots and correlation coefficients using all of the laser spot data (**Fig. 9**) show significant positive correlations between those elements regarded as being substituting ones (Ba vs Sr, Sr vs Mg), whilst significant negative correlations occur between elements deemed to be incompatible (U vs Mg, U vs Sr) (Reeder & Paquette 1990). This is consistent with the general notion of compositional zoning (Paquette & Reeder 1990).

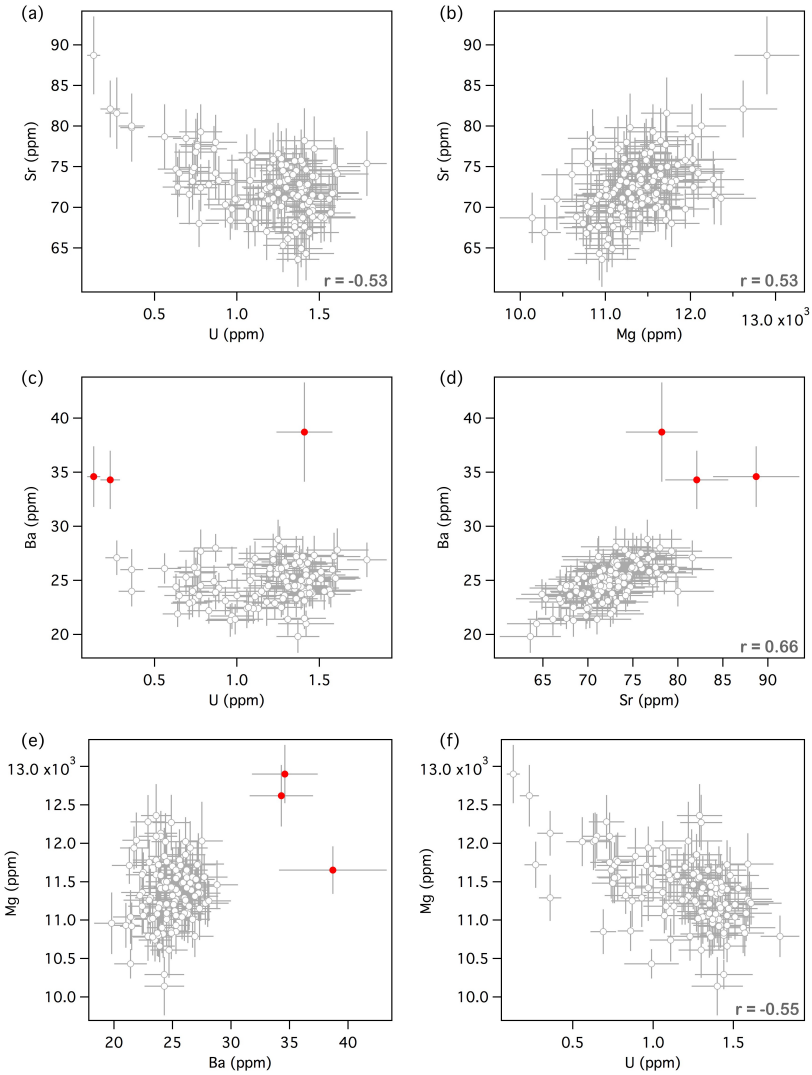

Figure 9: Scatterplots of all (n = 120) LA-ICP-MS calcite trace element spot data (Mg, Sr, Ba and U, all in ppm) shown in Figure 5. (a) Sr vs U; (b) Sr vs Mg; (c) Ba vs U; (d) Ba vs Sr; (e) Mg vs Ba; (f) Mg vs U. Error bars represent the measurement error from downhole ablation (2 s.e.). All Pearson *r* correlation coefficients shown are statistically significant at $p \leq 0.05$). Red symbols represent outlying Ba values excluded from all Ba vs X correlations.

The tendency for U to have the greatest heterogeneity (in terms of proportional variability around the mean value) is consistent with patterns observed in a 2D image of this element produced from the Marine Isotope Stage (MIS) 7 and 8 section of another core drilled from CD3 (Figure 2d in Drysdale et al. 2012). In this image, dendritic zones of low U are visible, with the range of U concentrations (0.6 to 1.6 ppm) similar to that shown in **Fig. 5**; a hint of Sr and Ba zoning in the same regions of this image is also apparent. This pattern in U has since been shown to persist from the core top (modern) back to at least the MIS 12 section (our unpublished data), and whilst lying beyond the scope of this present work, a future multi-element study warrants further investigation. Such 2D patterns may be linked to the variations observed in **Fig. 5**, and is suggestive of either petrographic or crystallographic control of U (and

potentially Sr and Ba) incorporation into calcite or selective leaching of U along specific crystal sectors.

In oxidising environments, such as those of Laghetto Basso, U is usually present in its hexavalent state U(VI) as the uranyl ion (UO_2^{2+}) (Langmuir 1978), which is capable of forming bonds with ligands commonly found in natural waters (e.g. CO_3^{2-}) (Reeder et al. 2001). These are thought to be incorporated into calcite through either coprecipitation or adsorption (e.g. via colloids). U speciation is highly sensitive to pH (Langmuir 1978). Processing of the pool water hydrochemistry data through the MINTEQ program reveals the presence of two dominant uranyl species: the neutral complex $Ca_2UO_2(CO_3)_{3(aq)}$ (~55-56%) and the anion $CaUO_2(CO3)_2^{2-}$ (~41-42%). One possible explanation for the wide range of U concentrations in time-equivalent calcite is the incorporation of both of these species, each according to a different D_U. However, the affinity of the neutral species for calcite is thought to be low because of the positive charge of a calcite surface at the pH of Laghetto Basso waters (Chen et al. 2016). This implicates the uranyl anion as the form most likely to be incorporated into CD3-12. Although adsorption onto colloidal phases might be possible (Hartland et al. 2014; Wassenburg et al. 2016), the long travel path that percolation waters take before reaching the GdS, and the low soil cover above the cave, would argue against a strong presence of colloids in the pool waters. This points to the direct incorporation of uranyl into the calcite, most likely by U^{6+} substitution for Ca^{2+} and two axial oxygen atoms substituting for the carbonate ion (Kelly et al. 2003).

5.4 Partition coefficients: comparison with previous studies

5.4.1 Introduction

We now compare our calcite partition coefficients for Mg, Sr, Ba and U with previously published values. Partition coefficients for calcite have been derived from a range of laboratory and natural settings (Huang & Fairchild 2001; Tremaine & Froelich 2013), representing a diversity of physico-chemical environments. For example, the strong interest in the study of trace elements in marine carbonates has seen many laboratory studies where calcite has been farmed from solutions that simulate seawater chemistry (Kitano & Oomori 1971; Mucci & Morse 1983; Burton & Walter 1991; Yoshimura et al. 2015; Chen et al. 2016). Given the relatively narrow range of hydrogeochemical conditions of most cave systems, the comparisons we make below are largely restricted to coefficients derived from field studies of caves (Holland et al. 1964; Gascoyne 1983; Huang et al. 2001; Karmann et al. 2007; Fairchild et al. 2010;

Tremaine & Froelich 2013) and cave-analogue laboratory studies (Huang & Fairchild 2001; Day & Henderson 2013) (**Table 5**).

An unavoidable problem of deriving calcite partition coefficients in cave studies is the stability of the solution [X/Ca] values at each monitoring station within the cave through the period of each calcite harvest. Source-water [X/Ca] values can change relatively rapidly (e.g. McDonald et al. 2004; Tremaine & Froelich 2013), and although it is common to average before and after (or more) values over the period of calcite growth, it is not possible to determine the weighting of each individual [X/Ca] value without some form of continuous monitoring, or at least very intensive (e.g. monthly) sampling. An additional potential problem in cave studies is whether or not farmed calcite (e.g. by precipitation onto glass plates) is truly representative of natural calcite growth, particularly in the context of crystal growth and morphology effects on element partitioning. This is also an issue for cave-analogue studies, which, like other related laboratory (e.g. seawater-analogue) experiments, suffer the additional problem of using synthetically prepared solutions. In this study, we have attempted to overcome these issues by targeting a very deep cave environment characterised by relatively stable hydrochemistry, and by sampling naturally grown calcite.

5.4.2 Magnesium

The D_{Mg} for Laghetto Basso (0.042 ± 0.002) is one the highest mean values ever recorded for cave or cave-analogue conditions, being exceeded in mean values only by Gascoyne (1983) in his study of Jamaican cave calcite (**Table 5**). Considering the thermodynamic tendency for D_{Mg} to vary positively with temperature (Katz 1973; Gascoyne 1983; Mucci & Morse 1983; Burton & Walter 1991; Huang & Fairchild 2001; Day & Henderson 2013), the high value is surprising given the relatively low temperatures of Laghetto Basso waters (~8 °C) and the expectation that during warmer periods (all other things being equal) the pool waters would produce even higher D_{Mg} values. Potential reasons for such a high D_{Mg} at this low temperature include the pool water [Mg/Ca], which is high for karst waters (~1.2). To examine this possibility further, we compared the Laghetto Basso D_{Mg} with data from a range of seawater or seawater-analogue studies, where the solution [Mg/Ca] reaches up to 20. As **Fig. 10** shows, the slopes of temperature vs D_{Mg} from these studies (Mucci 1987); Oomori et al. 1987; Burton and Walter 1991) fall within the scatter of temperature vs D_{Mg} for cave and cave-analogue studies, where [Mg/Ca] is <1, suggesting that [Mg/Ca] is not significant. Mucci & Morse (1983), however, report an increase in D_{Mg} from 0.012 to 0.027 at 25°C as the solution [Mg/Ca] decreases from

7.5 to 1, but an identical experiment conducted at Laghetto Basso temperatures using a solution [Mg/Ca] ≈1 would produce significantly *lower* D_{Mg} values given the temperature/D_{Mg} relationship. Therefore, we disqualify the high pool-water [Mg/Ca] as the reason for the unusually high Laghetto Basso D_{Mg}.

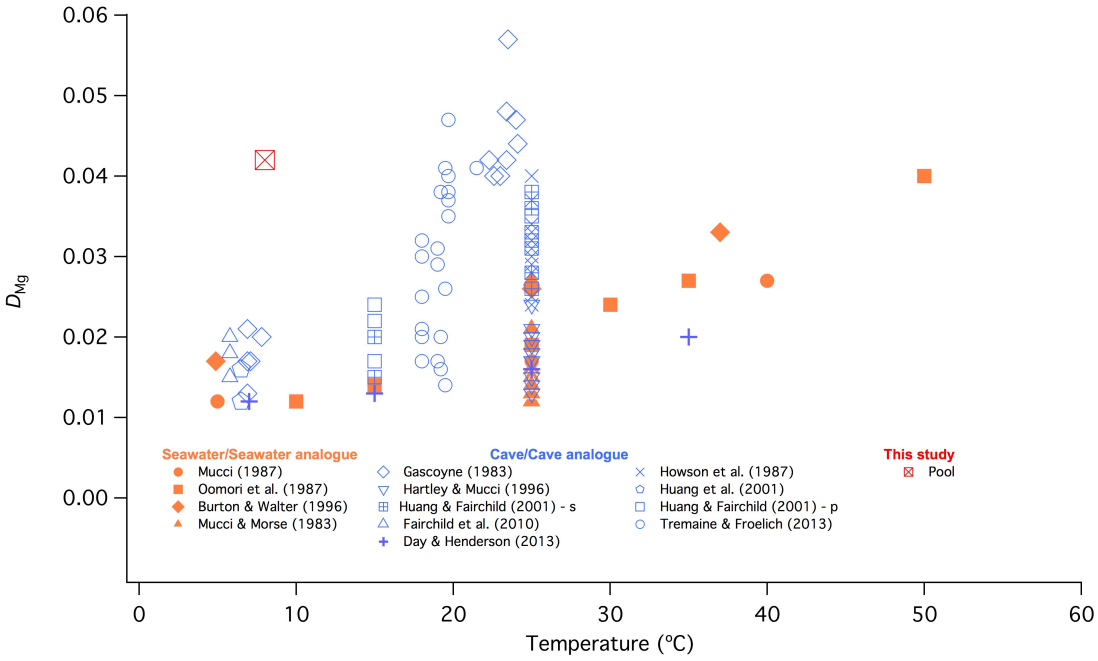

Figure 10: Comparison of D_{Mg} values versus temperature between a range of published cave/cave analogue (blue symbols) and seawater-analogue studies (orange symbols) and this study (red symbols). The straw (s) and plate (p) values are shown separately for the Huang & Fairchild (2001) data.

Source-water PCO_2 and saturation state, the reaction rate and crystal nucleation style have also been considered as possible drivers of D_{Mg} variations (Howson et al. 1987; Huang & Fairchild 2001; Hartley & Mucci 1996; Mavromatis et al. 2013), but these have been either rejected as having negligible influence (PCO_2) or their effects can be ruled out in the case of Laghetto Basso because the direction of D_{Mg} change is contrary to what would be expected. For example, homogeneous nucleation is thought to drive D_{Mg} values lower, but many experimental studies include crystal seeding (e.g. Huang & Fairchild 2001; Day & Henderson 2013) to mimic the heterogeneous nucleation observed in marine and cave settings. The results of cave-analogue experiments conducted in this way still yield D_{Mg} values much lower than Laghetto Basso at or near the observed pool temperatures. The effects of growth rate and saturation state were investigated recently by Mavromatis et al. (2013) at 25°C and 1 atm PCO_2, who found clear increases in D_{Mg} with both variables. However, these factors cannot explain the high D_{Mg} in Laghetto Basso calcite, given that the relatively low saturation state of the waters, and the very

low growth rates, plus cooler temperatures, would yield even higher D_{Mg} at the experimental conditions used by Mavromatis et al. (2013). In a study of a Florida cave, Tremaine and Froelich (2013) produced a detailed dataset of paired growth rates and D_{Mg} (and D_{Sr}) within a narrow range of cave temperatures (18 – 21.5°C), but despite a considerable range in coefficients, no relationship is observed.

The unusually high D_{Mg} value for Laghetto Basso calcite possibly owes its origin to the low-ionic strength and low-saturation-state of its source waters, which, in addition to the hydrodynamics of a subaqueous setting, give rise to the excessively slow growth rates of CD3. Such unusual conditions for a speleothem have not been encountered in previous cave and cave-analogue investigations. Recently, a comparison of modern calcite and pool waters from Laghetto Basso and Devils Hole (Nevada, USA) (Daëron et al. 2019) has suggested that the depositional conditions at these two sites are likely to approximate thermodynamic isotopic equilibrium, or at least closer to equilibrium compared to previous studies. Combining isotopic information from both sites across a temperature range spanning most speleothem settings (~8 and 34 ºC) produces calcite clumped-isotope calibration and conventional oxygen isotope fractionation curves that are significantly offset from those of calcites formed under different depositional conditions. Like Laghetto Basso, Devils Hole calcite growth rates are extremely slow on account of the hydrochemistry and hydrodynamic setting (Plummer et al. 2000). It would be useful to conduct future cave-analogue studies that mimic subaqueous environments like Laghetto Basso to examine D_{Mg} and other D_X across a range of growth rate, temperature and low-ionic-strength conditions.

5.4.3 Strontium

The mean D_{Sr} for Laghetto Basso (0.100 ± 0.007; **Table 4**) lies within the range of values observed in other cave studies. As with Mg, the partitioning of Sr into calcite has been the subject of considerable study in both natural and laboratory cave settings as well as marine applications (Böttcher & Dietzel 2010). The numerous possible factors driving D_{Sr} variations in marine studies have also been explored for speleothems, notably temperature, solution [Sr/Ca], [Mg/Ca] and [Na/Ca], and growth rate. In two detailed cave-analogue studies and one natural cave study, Fairchild & Huang (2001), Day & Henderson (2013) and Tremaine & Froelich (2013) each found no relationship between D_{Sr} and either growth rate or temperature. Huang & Fairchild (2001), however, concluded that the low Na concentrations used in their experimental solutions may have contributed to their D_{Sr} being higher than those from seawater-

analogue studies, where much higher Na concentrations are used. This is because the Na ion is thought to outcompete Sr for non-lattice sites on the calcite crystal (Pingitore & Eastman 1986). Although there has been no subsequent systematic study since Huang and Fairchild (2001) on the effects of solution [Na/Ca], [Sr/Ca] and [Mg/Ca] on D_{Sr} in cave or cave-analogue settings, the data presented in Tremaine & Froelich (2013) (their Supplementary Table EC.1) contain a sufficient spread of both solution [X/Ca] and D_{Sr} values to test this. Statistically significant negative correlations are found for [Na/Ca] versus D_{Sr} (r = -0.89) and [Sr/Ca] versus D_{Sr} (r = -0.77) (**Fig. 11a**); no significant correlation exists for [Mg/Ca] versus D_{Sr}. Although we do not have individual calcite-water [X/Ca] pairs to perform precisely the same test on the pool-water/CD3-12 data, we can see that the [Sr/Ca] versus D_{Sr} for CD3-12 (closed green diamonds, **Fig. 11a**) lies close to the scatter in the Tremaine & Froelich (2013) data. Further, the [Na/Ca] versus D_{Sr} for CD3-12 lie well clear of the corresponding Tremaine & Froelich (2013) values. Given the proposed effects of Na described above (Pingitore & Eastman 1986), the relatively high Na concentrations in Laghetto Basso should yield lower D_{Sr} if Na concentrations *per se* were important. A more robust test of the effects of Na is to use [Na/Sr] instead of [Na/Ca]: if Na outcompetes Sr for lattice sites then this should be evident in the ratio of these two elements. As shown in **Fig. 11b**, this is indeed the case: a significant negative exponential relationship exists between [Na/Sr] and D_{Sr} based on the data from Tremaine and Froelich (2013), and Day and Henderson (2013).

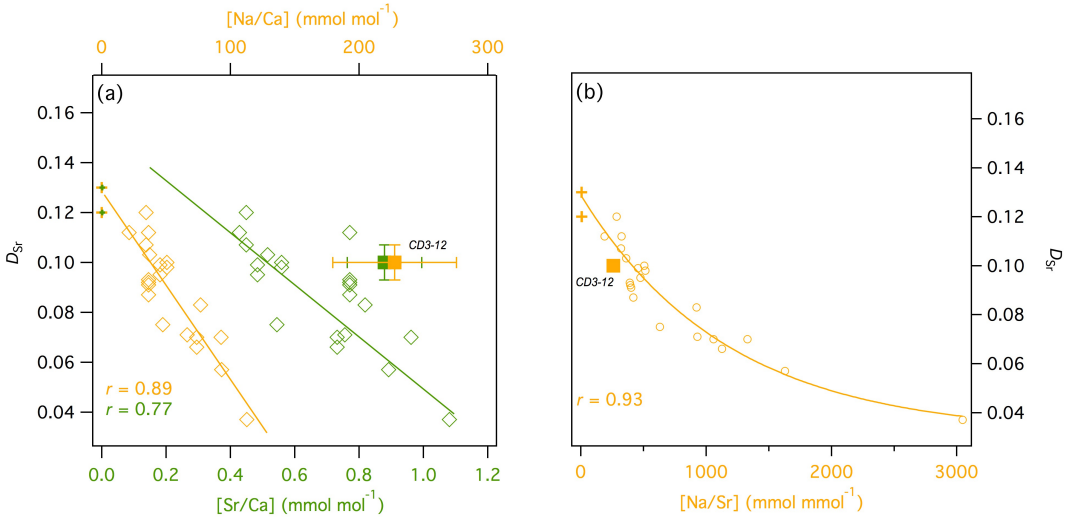

Figure 11: (a) Scatterplots of [Na/Ca] vs D_{Sr} (orange symbols) and [Sr/Ca] versus D_{Sr} (green symbols) for data presented in Tremaine and Froelich (2013) (open diamonds), Day and Henderson (2013) (crosses) and this study (CD3-12: solid squares). The Pearson r correlation coefficients are statistically significant (df = 19, p < 0.05) and correspond to the Tremaine and Froelich (2013) data only. (b) Scatterplot of [Na/Sr] vs D_{Sr} for the same studies shown in (a). The exponential fit, which models all data shown, is described by the equation $y = 0.1173e^{-0.0004x}$ and is statistically significant (df = 24, p < 0.05).

5.4.3 Barium and Uranium

The partitioning of Ba and U into calcite has not been the explicit subject of experimental cave investigations. The only cave-analogue study is that of Day and Henderson (2013), who reported a mean D_{Ba} value slightly larger than that for CD3-12. Although the study of Day and Henderson (2013) was conducted at temperatures (25° and 35°C) that are significantly higher than that of the Laghetto Basso water, temperature is not regarded as important in controlling D_{Ba} (Lea & Spero 1994). Growth rate and solution [Ba/Ca] have been linked to variations in D_{Ba} (Pingitore & Eastman 1984; Tesoriero & Pankow 1996), with higher growth rates producing higher D_{Ba}. However, these relationships have only been observed once growth rates and [Ba/Ca] greatly exceed those of CD3-12. Day and Henderson (2013) observed no relationship between growth rate and D_{Ba} (or D_U).

Uranium partitioning has been shown to vary with growth rate and temperature. The D_U values for CD3-12 (0.013 ± 0.002) are between 5 and 9 times below those experimentally determined by Day and Henderson (2013) (**Table 4**). They found a weak negative relationship between temperature and D_U, with values decreasing from 0.11 ± 0.011 to 0.062 ± 0.012 as temperature rose from 7°C to 35°C. However, the value for CD3-12 is almost an order of magnitude lower than Day and Henderson (2013) at similar temperatures.

Several studies have evaluated the effects of growth rate on D_U. Weremeichik et al. (2017) determined that D_U increased from 0.02 to 0.06 as growth rate increased from 0.01 to 0.14 nm s^{-1}. Although the Holocene growth rates observed in CD3-12 (1.24×10^{-5} nm s^{-1}) are several orders of magnitude lower than these, the direction of D_U change is consistent. Further, the starting solution [U/Ca] used by Weremeichik et al. (2017) (0.919 mmol/mol) is ~24 times higher than the Corchia pool water [U/Ca]. The much slower growth rates in the pool implies that the calcite crystals remain exposed to the solution for much longer before being 'protected' by further calcite growth. This would facilitate leaching or desorption of uranyl carbonate from the calcite lattice, given the high solubility of this species.

6. CONCLUSIONS

In this study, we have sought to advance understanding of how trace elements are incorporated into natural calcites by investigating the partitioning of Mg, Sr, Ba and U into subaqueous cave calcite, a rarely studied form of speleothem. We have shown that the pool-water chemistry of

Laghetto Basso displays decadal-scale stability, in contrast to percolation-waters reported in a number of other cave studies (e.g. Fairchild et al. 2000; McDonald et al. 2004; Tremaine & Froelich 2013). This produces relatively well-constrained solution [X/Ca] from which to derive D_X values. We have measured [X/Ca] on 'modern' subaqueous calcite (CD3-12) that grows naturally from these pool waters, rather than calcite grown on seeded, artificial substrata or from synthetic solutions under laboratory conditions.

Several lines of evidence indicate that the outer surface of CD3 is actively depositing today. These include a U-Th chronology corrected to an independently dated age profile of a stalagmite from the same cave chamber, the supersaturated state of the pool water, and the fact that the speleothem has grown over multiple glacial-interglacial cycles (Drysdale et al. 2012). The slow growth rates of CD3-12, the challenge of sampling its active outer growth surface, and the potential for time-equivalent layers of non-uniform thickness prevent us from unequivocally determining that the calcite grew exclusively across the monitoring period. However, the stability of the pool-water chemistry over a 15-year period (1997 to 2012) suggests at least decadal-scale hydrochemical stability, conducive to precipitating relatively invariant calcite [X/Ca]. This is validated by the statistically indistinguishable mean CD3-12 [X/Ca] values from the surface (analysed by solution ICP-MS and incorporating, no more than ~300 years of growth) and the outermost 7 μm of calcite (analysed by LA-ICP-MS and incorporating ~21 years of growth). Taking these solution and calcite results together, we have circumvented the issue of having to average (often quite different) instantaneous solution [X/Ca] values for pairing with the [X/Ca] from calcite grown over the same period. We argue that the mean D_X values from CD3-12 therefore represent reliable estimates of partition coefficients from naturally grown subaqueous calcite.

Comparison with published studies reveals that the mean D_{Mg} value from CD3-12 is significantly higher than values produced from other cave and cave-analogue (and indeed, sea-water analogue) situations given the low pool-water temperature. This may be facilitated by the extremely slow growth rates of the speleothem. Future calcite/source-water studies conducted in broadly similar cave-pool settings but at sites with different temperatures, could enable quantification of D_{Mg}-temperature relationships. However, we suspect that finding appropriate sites (dolomitic bedrock, low-ionic strength waters, deep-set cavern) would prove rather challenging, and laboratory simulations might be the most appropriate approach in this regard.

The D_{Sr} values for CD3-12 are comparable with published cave/cave analogue studies, the few data available suggest that [Na/Sr] might be an important factor in controlling Sr partitioning through Na outcompeting Sr for compatible non-lattice sites. The long exposure time of the CD3-12 calcite surface, where growth rates are a mere ~0.3 – 0.4 μm per year (averaged over the Holocene), raises the prospect of dissolution of soluble uranyl carbonate. This could explain the higher variability of U partitioning and low mean D_U shown here, as well as the dendritic zones of low U concentration observed throughout the upper half of CD3-12, including the MIS 8-7 section reported in Drysdale et al. (2012).

In spite of the relatively well-constrained D_X values obtained, data from both the surface calcite and the outermost 7 μm reveal heterogeneity in trace element distribution in CD3-12, which, as expected, is more evident in the better-resolved laser data. A number of the laser profiles show covariation amongst elements, suggesting that element incorporation may be influenced by compositional zoning or fabric effects. Mapping the spatial patterns of elemental variation in 2D is necessary to determine the presence / extent of compositional zoning. It would enable the quantification of the range of elemental concentrations, and reveal if zoning bears any relationship to the prevailing climate state, upon which speleothem growth rates and hydrochemistry depend.

Single subaqueous speleothems can preserve continuous palaeoclimate records spanning many hundreds of thousands of years (Winograd et al. 1992). The subaqueous speleothem used in the present study captures a palaeoclimate record spanning almost the last one million years (Drysdale et al. 2012). As demonstrated by previous research on stalagmites and flowstones (Drysdale et al. 2006; Johnson et al. 2006; Wong et al. 2011; Hartmann et al. 2013; Weber et al. 2018), trace-element changes have the potential to complement stable-isotope records from this speleothem, and to play a key role in developing robust interpretations of regional palaeoclimate and wider environmental changes (e.g. long-term landscape evolution) over multiple glacial-interglacial cycles. The current study has laid the foundations for additional extensive trace element study of CD3 by deriving partitioning coefficients under modern conditions. Future work will focus on long-term trace element changes and the palaeoclimate drivers, particularly whether elements considered to be useful hydrological tracers from previous speleothem studies also preserve palaeohydrological information in CD3. However, given the slow growth rates and relatively complacent decadal-scale hydrochemistry,

palaeohydrological changes would likely only be resolved at centennial or greater (e.g. millennial or orbital) time scales.

ACKNOWLEDGEMENTS

This research was supported by funding from the Australian Research Council (Discovery Project number DP160102969, awarded to RD, GZ, ER and JW; Laureate Fellowship FL160100028 awarded to JW; and Future Fellowship FT130100801 awarded to JH. We are grateful to the Gruppo Speleologico Lucchese and the Federazione Speleologica Toscana for outstanding support. This paper benefitted from discussions with Professor Richard Reeder. This paper has benefitted significantly from three very meticulous and constructive reviews, for which we are very grateful.

REFERENCES

Azzaro, E., Negretti, G. and Tucci, P. (1987) A chemiostratigraphic study of the metadolomitic sequence of the southern side of Mount Corchia (Alpi Apuane, Italy). *Geologica Rom.* 26, 293-303.

Bajo, P., Drysdale, R.N., Woodhead, J.D., Hellstrom, J.C., Zanchetta, G. 2012. High-resolution U-Pb dating of an Early Pleistocene stalagmite from Corchia Cave (central Italy). *Quatern. Geochronology* 14, 5-17.

Bajo, P., Borsato, A., Drysdale, R., Hua, Q., Frisia, S., Zanchetta, G., Hellstrom, J. and Woodhead, J. (2017) Stalagmite carbon isotopes and dead carbon proportion (DCP) in a near-closed-system situation: An interplay between sulphuric and carbonic acid dissolution. *Geochim. Cosmochim. Acta* 210, 208-227.

Bajo, P., Hellstrom, J., Frisia, S., Drysdale, R., Black, J., Woodhead, J., Borsato, A., Zanchetta, G., Wallace, M.W., Regattieri, E. and Haese, R. (2016) "Cryptic" diagenesis and its implications for speleothem geochronologies. *Quatern. Sci. Rev.* 148, 17-28.

Balboni, E., Morrison, J.M., Wang, Z., Engelhard, M.H. and Burns, P.C. (2015) Incorporation of Np(V) and U(VI) in carbonate and sulfate minerals crystallized from aqueous solution. *Geochim. Cosmochim. Acta* 151, 133-149.

Baneschi, I., Piccini, L., Regattieri, E., Isola, I., Guidi, M., Lotti, L., Mantelli, F., Menichetti, M., Drysdale, R.N. and Zanchetta, G. (2011) Hypogean microclimatology and hydrology of the 800-900 m asl level in the Monte Corchia cave (Tuscany, Italy): preliminary considerations and implications for paleoclimatological studies. *Acta Carsologica* 40, 175-187.

Bernal, J.P., Cruz, F.W., Stríkis, N.M., Wang, X., Deininger, M., Catunda, M.C.A., Ortega-Obregón, C., Cheng, H., Edwards, R.L. and Auler, A.S. (2016) High-resolution Holocene South American monsoon history recorded by a speleothem from Botuverá Cave, Brazil. *Earth and Planetary Science Letters* 450, 186-196.

Borsato, A., Frisia, S., Fairchild, I.J., Somogyi, A. and Susini, J. (2007) Trace element distribution in annual stalagmite laminae mapped by micrometer-resolution X-ray fluorescence: Implications for incorporation of environmentally significant species. *Geochim. Cosmochim. Acta* 71, 1494-1512.

Böttcher, M.E. and Dietzel, M. (2010) Metal-ion partitioning during low-temperature precipitation and dissolution of anhydrous carbonates and sulphates. *EMU Notes in Mineralogy* 10, 139-187.

Bourdin, C., Douville, E. and Genty, D. (2011) Alkaline-earth metal and rare-earth element incorporation control by ionic radius and growth rate on a stalagmite from the Chauvet Cave, Southeastern France. *Chem. Geol.* 290, 1-11.

Burton, E.A. and Walter, L.M. (1991) The effects of P_{CO2} and temperature on magnesium incorporation in calcite in seawater and $MgCl_2$-$CaCl_2$ solutions. *Geochim. Cosmochim. Acta* 55, 777-785.

Busenberg, E. and Niel Plummer, L. (1989) Thermodynamics of magnesian calcite solid-solutions at 25°C and 1 atm total pressure. *Geochim. Cosmochim. Acta* 53, 1189-1208.

Busenberg, E. and Plummer, N. (1982) The kinetics of dissolution of dolomite in CO_2-H_2O systems at 1.5 to 65°C and 0 to 1 atm PCO_2. *Amer. J. Sci.* 282, 45-78.

Carmignani, L. and Giglia, G. (1984) "Autoctono Apuano" e Falda Toscana. Sintesi dei dati e delle interpretazionini, Cento anni di Geologia Italiana. Pitagora, Bologna, pp. 199-214.

Carmignani, L. and Kligfield, R. (1990) Crustal extension in the northern Apennines: The transition from compression to extension in the Alpi Apuane Core Complex. *Tectonics* 9, 1275-1303.

Casteel, R.C. and Banner, J.L. (2015) Temperature-driven seasonal calcite growth and drip water trace element variations in a well-ventilated Texas cave: Implications for speleothem paleoclimate studies. *Chem. Geol.* 392, 43-58.

Chen, X., Romaniello, S.J., Herrmann, A.D., Wasylenki, L.E., Anbar, A.D. (2016) Uranium isotope fractionation during coprecipitation with aragonite and calcite. *Geochim. Cosmochim. Acta* 188, 189-207.

Cheng, H., Edwards, R.L., Broecker, W.S., Denton, G.H., Kong, X., Wang, Y., Zhang, R. and Wang, X. (2009) Ice age terminations. *Science* 326, 248-252.

Cheng, H., Edwards, R.L., Sinha, A., Spötl, C., Yi, L., Chen, S., Kelly, M., Kathayat, G., Wang, X., Li, X., Kong, X., Wang, Y., Ning, Y. and Zhang, H. (2016) The Asian monsoon over the past 640,000 years and ice age terminations. *Nature* 534, 640-648.

Conti, P., Di Pisa, A., Gattiglio, M. and Meccheri, M. (1993) The Pre-Alpine Basement in the Alpi Apuane (Northern Apennines, Italy), in: von Raumer, J.F., Neubauer, F. (Eds.), *Pre-Mesozoic Geology in the Alps*. Springer Berlin Heidelberg, Berlin, Heidelberg, pp. 609-621.

Cortecci, G., Dinelli, E., Indrizzi, M.C., Susini, C. and Adorni Braccesi, A. (1999) The Apuane Alps metamorphic complex, Northern Tuscany: chemical and isotopic features of Grezzoni and Marmi dolomitici. *Atti Soc. Tosc. Sci. Nat., Mem.*, Serie A 106, 79-89.

Cruz, F.W., Burns, S.J., Jercinovic, M., Karmann, I., Sharp, W.D. and Vuille, M. (2007) Evidence of rainfall variations in Southern Brazil from trace element ratios (Mg/Ca and Sr/Ca) in a Late Pleistocene stalagmite. *Geochim. Cosmochim. Acta* 71, 2250-2263.

Daeron, M., Drysdale, R., Peral, M., Huyghe, D., Blamart, D., Coplen, T., Lartud, F. & Zanchetta, G. (2019) Most Earth-surface calcites precipitated out of isotopic equilibrium. *Nature Communications* doi.org/10.1038/s41467-019-08336-5.

Day, C.C. and Henderson, G.M. (2013) Controls on trace-element partitioning in cave-analogue calcite. *Geochim. Cosmochim. Acta* 120, 612-627.

Drysdale, R.N. (2001) Factors controlling the hydrochemistry of Louie Creek, a travertinedepositing stream in the seasonally wet tropics of northern Australia. *Mar. Freshwater Res.* 52, 793-804.

Drysdale, R., Zanchetta, G., Hellstrom, J.C., Zhao, J-x, Fallick, A.C., Isola, I., Bruschi, G. (2004) Palaeoclimatic implications of the growth history and stable isotope ($\delta^{18}O$ and $\delta^{13}C$) geochemistry of a Middle to Late Pleistocene stalagmite from central-western Italy. *Earth and Planetary Science Letters* 227, 215-229.

Drysdale, R.N., Zanchetta, G., Hellstrom, J.C., Fallick, A.E. and Zhao, J.X. (2005) Stalagmite evidence for the onset of the Last Interglacial in southern Europe at 129 ± 1 ka. *Geophys. Res. Lett.* 32, L24708, doi:24710.21029/22005GL024658.

Drysdale, R.N., Zanchetta, G., Hellstrom, J., Maas, R., Fallick, A., Pickett, M., Cartwright, I. and Piccini, L. (2006) Late Holocene drought responsible for the collapse of Old World civilizations is recorded in an Italian cave flowstone. *Geology* 34, 101-104.

Drysdale, R., Hellstrom, J., Couchoud, I., Zanchetta, G., Woodhead, J., Greig, A., Fallick, A., Isola, I. (2008) Towards a new radiometrically dated North Atlantic palaeo-climate record covering the last million years: preliminary results from Corchia Cave speleothems, Italy. European Geosciences Union abstract EGU2008-A-05940.

Drysdale R. N., Paul B. T., Hellstrom J. C., Couchoud I., Greig A., Bajo P., Zanchetta G., Isola I., Spötl C., Baneschi I., Regattieri, E. and Woodhead J. D. (2012) Precise microsampling of poorly laminated speleothems for U-series dating. *Quat. Geochronol.* 14, 38–47.

Edwards, R.L., Gallup, C.D., Ludwig, K.R., Simmons, K.R., Winograd, I.J., Szabo, B.J. and Riggs, A.C. (1993) Dating of the Devils Hole calcite vein. *Science* 259, 1626-1627.

Fairchild, I.J. and Baker, A. (2012) *Speleothem science: From process to past environments*. Wiley-Blackwell.

Fairchild, I.J., Baker, A., Borsato, A., Frisia, S., Hinton, R.W., McDermott, F. and Tooth, A.F. (2001) Annual to sub-annual resolution of multiple trace-element trends in speleothems. *J. Geol. Soc.* 158, 831-841.

Fairchild, I.J., Borsato, A., Tooth, A.F., Frisia, S., Hawkesworth, C.J., Huang, Y., McDermott, F. and Spiro, B. (2000) Controls on trace element (Sr-Mg) compositions of carbonate cave waters: implications for speleothem climatic records. *Chem. Geol.* 166, 255-269.

Fairchild, I.J., Spötl, C., Frisia, S., Borsato, A., Susini, J., Wynn, P.M. and Cauzid, J. (2010) Petrology and geochemistry of annually laminated stalagmites from an Alpine cave (Obir, Austria): seasonal cave physiology. *Geol. Soc. London, Spec. Pub.* 336, 295-321.

Fairchild, I.J. and Treble, P.C. (2009) Trace elements in speleothems as recorders of environmental change. *Quatern. Sci. Rev.* 28, 449-468.

Fohlmeister, J., Schröder-Ritzrau, A., Scholz, D., Spötl, C., Riechelmann, D.F.C., Mudelsee, M., Wackerbarth, A., Gerdes, A., Riechelmann, S., Immenhauser, A., Richter, D.K. and Mangini, A. (2012) Bunker Cave stalagmites: An archive for central European Holocene climate variability. *Climate of the Past* 8, 1751-1764.

Frisia, S. (2015) Microstratigraphic logging of calcite fabrics in speleothems as tool for palaeoclimate studies. *Int. J. Speleol.* 44, 1-16.

Gascoyne, M. (1983) Trace element partition coefficients in the calcite-water system and their paleoclimatic significance in cave studies. *J. Hydrol* 61, 213-222.

Gran, G. (1952) Determination of the equivalence point in potentiometric titrations. Part II. *Analyst* 77, 661-671.

Genty, D. & Massault, M. (1999) Carbon transfer dynamics from bomb 14C and d13C times series of a laminated stalagmite from SW France: modelling and comparison with other stalagmites. *Geochimica et Cosmochimica Acta* 63, 1537–1548.

Griffiths, M., Drysdale, R., Gagan, M., Zhao, J-x., Ayliffe, L., Hantoro, W., Frisia, S., Hellstrom, J., Fischer, M. Feng, J-x., Suwargadi, B. (2010). Multi-proxy stalagmite evidence for east Indonesian monsoon variability during the Holocene. *Earth and Planetary Science Letters* 292, 27-38.

Griffiths, M.L., Fohlmeister, J., Drysdale, R.N., Hua, Q., Johnson, K.R., Hellstrom, J.C., Gagan, M.K., Zhao, J-x. 2012. Hydrological control on the dead-carbon content of a Holocene tropical speleothem. *Quatern. Geochronology* doi:10.1016/j.quageo.2012.04.001.

Hartland, A., Fairchild, I.J., Müller, W. and Dominguez-Villar, D. (2014) Preservation of NOM-metal complexes in a modern hyperalkaline stalagmite: Implications for speleothem trace element geochemistry. *Geochim. Cosmochim. Acta* 128, 29-43.

Hartley, G. and Mucci, A. (1996) The influence of P_{CO2} on the partitioning of magnesium in calcite overgrowths precipitated from artificial seawater at 25° and 1 atm total pressure. *Geochim. Cosmochim. Acta* 60, 315-324.

Hartmann, A., Eiche, E., Neumann, T., Fohlmeister, J., Schröder-Ritzrau, A., Mangini, A. and Haryono, E. (2013) Multi-proxy evidence for human-induced deforestation and cultivation from a late Holocene stalagmite from middle java, Indonesia. Chemical Geology 357, 8-17.

Hellstrom, J. and McCulloch, M. (2000) Multi-proxy constraints on the climatic significance of trace element records from a New-Zealand speleothem. *Earth Planet. Sci. Lett.* 179, 287-297.

Hellstrom, J., Paton, C., Woodhead, J. and Hergt, J. (2008) Iolite: software for spatially resolved LA-(quad and MC) ICPMS analysis, in: Sylvester, P. (Ed.), *Laser Ablation ICP–MS in the Earth Sciences: Current Practices and Outstanding Issues*, pp. 343-348.

Hendy, C.H. and Wilson, A.T. (1968) Palaeoclimatic data from speleothems. *Nature* 219, 48-51.

Hodge, E., McDonald, J., Fischer, M., Redwood, D., Hua, Q., Levchenko, V., Drysdale, R., Waring, C. & Fink, D. (2011) Using the ^{14}C bomb pulse to date young speleothems. *Radiocarbon* 53, 345-357.

Holland, H.D., Holland, H.J. and Munoz, J.L. (1964) The coprecipitation of cations with CaCO3-II. The coprecipitation of Sr^{2+} with calcite between 90° and 100°C. *Geochim. Cosmochim. Acta* 28, 1287-1301.

Howson, M.R., Pethybridge, A.D. and House, W.A. (1987) Synthesis and distribution coefficient of low-magnesium calcites. *Chem. Geol.* 64, 79-87.

Huang, Y. and Fairchild, I.J. (2001) Partitioning of Sr^{2+} and Mg^{2+} into calcite under karst-analogue experimental conditions. *Geochim. Cosmochim. Acta* 65, 47-62.

Huang, Y.M., Fairchild, I.J., Borsato, A., Frisia, S., Cassidy, N.J., McDermott, F. and Hawkesworth, C.J. (2001) Seasonal variations in Sr, Mg and P in modern speleothems (Grotta di Ernesto, Italy). *Chem. Geol.* 175, 429-448.

Isola, I, Zanchetta, G, Drysdale, RN, Regattieri, E, Bini, M, Bajo, P, Hellstrom, JC, Baneschi, I, Lionello, P, Woodhead, J & Greig, A. (2019) The 4.2-ka event in the central

Mediterranean: new data from a Corchia speleothem (Apuan Alps, central Italy). *Climate of the Past* 15, 135–151, doi:10.5194/cp-15-135-2019.

Johnson, K.R., Hu, C., Belshaw, N.S. & Henderson, G.M. (2006) Seasonal trace-element and stable isotope variations in a Chinese speleothem: the potential for high-resolution paleomonsoon reconstruction. *Earth and Planetary Science Letters* 244, 394–407.

Karmann, I., Cruz, F.W., Viana, O. and Burns, S.J. (2007) Climate influence on geochemistry parameters of waters from Santana–Pérolas cave system, Brazil. *Chem. Geol.* 244, 232-247.

Katz, A. (1973) The interaction of magnesium with calcite during crystal growth at 25-90°C and one atmosphere. *Geochim. Cosmochim. Acta* 37, 1563-1586.

Kelly, S.D., Newville, M.G., Cheng, L., Kemner, K.M., Sutton, S.R., Fenter, P., Sturchio, N.C. and Spötl, C. (2003) Uranyl incorporation in natural calcite. *Environ. Sci. Technol.* 37, 1284-1287.

Kelly, S.D., Rasbury, E.T., Chattopadhyay, S., Kropf, A.J. and Kemner, K.M. (2006) Evidence of a stable uranyl site in ancient organic-rich calcite. *Environ. Sci. Technol.* 40, 2262-2268.

Kitano, Y. and Oomori, T. (1971) The coprecipitation of uranium with calcium carbonate. *J. Ocean. Soc. Japan* 27, 34-42.

Kligfield, R., Hunziker, J., Dallmeyer, R.D. and Schamel, S. (1986) Dating of deformation phases using K-Ar and $^{40}Ar/^{39}Ar$ techniques: results from the northern apennines. *J. Struct. Geol.* 8, 781-798.

Kolesar, P.T. and Riggs, A.C. (2004) Influence of depositional environment on Devils Hole calcite morphology and petrology, in: Sasowsky, I.D., Mylroie, J. (Eds.), *Studies of Cave Sediments*. Springer, Boston, MA, pp. 227-241.

Lachniet, M.S. (2009) Climatic and environmental controls on speleothem oxygen-isotope values. *Quatern. Sci. Rev.* 28, 412-432.

Langmuir, D. (1978) Uranium solution-mineral equilibria at low temperatures with applications to sedimentary ore deposits. *Geochim. Cosmochim. Acta* 42, 547-569.

Lauritzen, S.E. and Lundberg, J. (1999) Speleothems and climate: a special issue of *The Holocene*. *The Holocene* 9, 643-647.

Lea, D.W. and Spero, H.J. (1994) Assessing the reliability of paleochemical tracers: Barium uptake in the shells of planktonic foraminifera. *Paleocean.* 9, 445-452.

Liu, Y.H., Henderson, G.M., Hu, C.Y., Mason, A.J., Charnley, N., Johnson, K.R. and Xie, S.C. (2013) Links between the East Asian monsoon and North Atlantic climate during the 8,200 year event. *Nature Geoscience* 6, 117-120.

Markowska, M., Baker, A., Andersen, M.S., Jex, C.N., Cuthbert, M.O., Rau, G.C., Graham, P.W., Rutlidge, H., Mariethoz, G., Marjo, C.E., Treble, P.C. and Edwards, N. (2016) Semi-arid zone caves: Evaporation and hydrological controls on $\delta^{18}O$ drip water composition and implications for speleothem paleoclimate reconstructions. *Quatern. Sci. Rev.* 131, 285-301.

Mattey, D., Lowry, D., Duffet, J., Fisher, R., Hodge, E. and Frisia, S. (2008) A 53-year seasonally resolved oxygen and carbon isotope record from a modern Gibraltar speleothem: Reconstructed drip water and relationship to local precipitation. *Earth Planet. Sci. Lett.* 269, 80-95.

Mattey, D.P., Fairchild, I.J., Atkinson, T.C., Latin, J.-P., Ainsworth, M. and Durell, R. (2010) Seasonal microclimate control of calcite fabrics, stable isotopes and trace elements in modern speleothem from St Michaels Cave, Gibraltar. *Geol. Soc., London, Spec. Pub.* 336, 323-344.

Mavromatis, V., Gautier, Q., Bosc, O. and Schott, J. (2013) Kinetics of Mg partition and Mg stable isotope fractionation during its incorporation in calcite. *Geochim. Cosmochim. Acta* 114, 188-203.

McDermott, F. (2004) Paleo-climate reconstruction from stable isotope variations in speleothems: a review. *Quatern. Sci. Rev.* 23, 901□918.

McDonald, J., Drysdale, R. and Hill, D. (2004) The 2002-2003 El Niño recorded in Australian cave drip waters: Implications for reconstructing rainfall histories using stalagmites. *Geophys. Res. Lett.* 31, doi:10.1029/2004GL020859.

McDonald, J., Drysdale, R., Hill, D., Chisari, R. and Wong, H. (2007) The hydrochemical response of cave drip waters to sub-annual and inter-annual climate variability, Wombeyan Caves, SE Australia. *Chem. Geol.* 244, 605-633.

Moseley, G.E., Edwards, R.L., Wendt, K.A., Cheng, H., Dublyansky, Y., Lu, Y., Boch, R. and Spötl, C. (2016) Reconciliation of the Devils Hole climate record with orbital forcing. *Science* 351, 165-168.

Mucci, A. and Morse, J.W. (1983) The incorporation of Mg^{2+} and Sr^{2+} into calcite overgrowths: influences of growth rate and solution composition. *Geochim. Cosmochim. Acta* 47, 217-233.

Mucci, A. (1987) Influence of temperature on the composition of magnesian calcite overgrowths precipitated from seawater. *Geochim. Cosmochim. Acta* 51, 1977-1984.

Neuser, R. D., Richter, D.K. (2007) Non-marine radiaxial fibrous calcites - examples of speleothems proved by electron backscatter diffraction. *Sed. Geol.* 194, 149-154.

Nielsen, M.R., Sand, K.K., Rodriguez-Blanco, J.D., Bovet, N., Generosi, J., Dalby, K.N. and Stipp, S.L.S. (2016) Inhibition of Calcite Growth: Combined Effects of Mg^{2+} and SO_4^{2-}. Crystal *Growth & Design* 16, 6199-6207.

Oomori, T., Kaneshima, H. and Maezato, Y. (1987) Distribution coefficient of Mg^{2+} ions between calcite and solution at 10-50°C. *Mar. Chem.* 20, 327-336.

Orland, I.J., Burstyn, Y., Bar-Matthews, M., Kozdon, R., Ayalon, A., Matthews, A. and Valley, J.W. (2014) Seasonal climate signals (1990-2008) in a modern Soreq Cave stalagmite as revealed by high-resolution geochemical analysis. Chemical Geology 363, 322-333.

Owen, R.A., Day, C.C, Hu, C.-Y., Liu, Y.-H., Pointing, M.D., Blättler, C.L. and Henderson, G.M. (2016) Calcium isotopes in caves as a proxy for aridity: modern calibration and application to the 8.2 kyr event. *Earth and Planetary Science Letters* 443, 129–138.

Paquette, J. and Reeder, R.J. (1995) Relationship between surface structure, growth mechanism, and trace element incorporation in calcite. *Geochim. Cosmochim. Acta* 59, 735-749.

Paton, C., Hellstrom, J., Paul, B., Woodhead, J. and Hergt, J. (2011) Iolite: Freeware for the visualisation and processing of mass spectrometric data. *J. Anal. At. Spectrom.* 26, 2508-2518.

Piccini, L., Zanchetta, G., Drysdale, R.N., Hellstrom, J., Isola, I., Fallick, A.E., Leone, G., Doveri, M., Mussi, M., Mantelli, F., Molli, G., Lotti, L., Roncioni, A., Regattieri, E., Meccheri, M. and Vaselli, L. (2008) The environmental features of the Monte Corchia cave system (Apuan Alps, central Italy) and their effects on speleothem growth. *Int. J. Speleol.* 37 153-172.

Pingitore, N.E. and Eastman, M.P. (1984) The experimental partitioning of Ba^{2+} into calcite. *Chem. Geol.* 45, 113-120.

Pingitore, N.E. and Eastman, M.P. (1986) The coprecipitation of Sr^{2+} with calcite at 25°C and 1 atm. *Geochim. Cosmochim. Acta* 50, 2195-2203.

Plummer, N., Busenberg, E., Riggs, A.C. (2000) In-situ growth of calcite at Devils Hole, Nevada: comparison of field and laboratory rates to a 500,000 year record of near-equilibrium calcite growth. *Aqueous Geochemistry* 6, 257-274.

Reed, M.H. (1982) Calculation of multicomponent chemical equilibria and reaction processes in systems involving minerals, gases and an aqueous phase. *Geochim. Cosmochim. Acta* 46, 513-528.

Reeder, R.J. and Grams, J.C. (1987) Sector zoning in calcite cement crystals: Implications for trace element distributions in carbonates. *Geochim. Cosmochim. Acta* 51, 187-194.

Reeder, R.J., Nugent, M., Beck, K.M., Tait, C.D., Hess, W.P., Morris, D.E., Heald, S.M. and Lanzirotti, A. (2001) Coprecipitation of Uranium(VI) with Calcite: XAFS, micro-XAS, and luminescence characterization. *Geochim. Cosmochim. Acta* 65, 3491–3503.

Reeder, R.J. and Paquette, J. (1990) Sector zoning in natural and synthetic calcites. *Sed. Geol.* 65, 239-247.

Reiners, P.W., Carlson, R.W., Renne, P.R., Cooper, K.M., Granger, D.E., McLean, N.M. and Schoene, B. (2017) *Geochronology and Thermochronology*. Wiley.

Richards, D.A. and Dorale, J.A. (2003) Uranium-series chronology and environmental applications of speleothems. *Rev. Mineral. Geochem.* 52, 407-460.

Rimstidt, J.D., Balog, A. and Webb, J. (1998) Distribution of trace elements between carbonate minerals and aqueous solutions. *Geochim. Cosmochim. Acta* 62, 1851-1863.

Schwarcz, H.P., Harmon, R.S., Thompson, P. and Ford, D.C. (1976) Stable isotope studies of fluid inclusions in speleothems and their paleoclimatic significance. *Geochim. Cosmochim. Acta* 40, 657-665.

Spötl, C. and Mattey, D. (2012) Scientific drilling of speleothems - a technical note. *Int. J. Speleol.* 41, 29-34.

Tesoriero, A.J. and Pankow, J.F. (1996) Solid solution partitioning of Sr^{2+}, Ba^{2+}, and Cd^{2+} to calcite. *Geochim. Cosmochim. Acta* 60, 1053-1063.

Treble, P., Chappell, J., Gagan, M., McKeegan, K. and Harrison, T. (2005) In situ measurement of seasonal $\delta^{18}O$ variations and analysis of isotopic trends in a modern speleothem from southwest Australia. *Earth Planet. Sci. Lett.* 233, 17-32.

Treble, P.C., Bradley, C., Wood, A., Baker, A., Jex, C.N., Fairchild, I.J., Gagan, M.K., Cowley, J. and Azcurra, C. (2013) An isotopic and modelling study of flow paths and storage in Quaternary calcarenite, SW Australia: implications for speleothem paleoclimate records. *Quatern. Sci. Rev.* 64, 90-103.

Tremaine, D.M. and Froelich, P.N. (2013) Speleothem trace element signatures: A hydrologic geochemical study of modern cave dripwaters and farmed calcite. *Geochim. Cosmochim. Acta* 121, 522-545.

Ünal-Imer, E., Shulmeister, J., Zhao, J.X., Uysal, I.T. and Feng, Y.X. (2016) High-resolution trace element and stable/radiogenic isotope profiles of late Pleistocene to Holocene

speleothems from Dim Cave, SW Turkey. *Palaeogeography, Palaeoclimatology, Palaeoecology* 452, 68-79.

Wassenburg, J.A., Scholz, D., Jochum, K.P., Cheng, H., Oster, J., Immenhauser, A., Richter, D.K., Häger, T., Hoffmann, D.L., Breitenbach, S.F.M., 2016. Determination of aragonite trace element partition coefficients from speleothem calcite-aragonite transitions. *Geochim. Cosmochim. Acta* 190, 347-367.

Weber, M., Scholz, D., Schröder-Ritzrau, A., Deininger, M., Spötl, C., Lugli, F., Mertz-Kraus, R., Jochum, K.P., Fohlmeister, J., Stumpf, C.F. and Riechelmann, D.F.C. (2018) Evidence of warm and humid interstadials in central Europe during early MIS 3 revealed by a multi-proxy speleothem record. *Quaternary Science Reviews* 200, 276-286.

Weremeichik, J.M., Gabitov, R.I., Thien, B.M.J. and Sadekov, A. (2017) The effect of growth rate on uranium partitioning between individual calcite crystals and fluid. *Chem. Geol.* 450, 145-153.

Winograd, I.J., Coplen, T.B., Landwehr, J.M., Riggs, A.C., Ludwig, K.R., Szabo, B.J., Kolesar, P.T. and Revesz, K.M. (1992) Continuous 500.000-year climate record from vein calcite in Devils Hole, Nevada. *Science* 258, 255-260.

Wong, C.I., Banner, J.L. and Musgrove, M. (2015) Holocene climate variability in Texas, USA: An integration of existing paleoclimate data and modeling with a new, high-resolution speleothem record. Quaternary Science Reviews 127, 155-173.

Woodhead, J., Hellstrom, J., Maas, R., Drysdale, R., Zanchetta, G., Devine, P. and Taylor, E. (2006) U-Pb geochronology of speleothems by MC-ICPMS. *Quat. Geochronol.* 1, 208-221.

Woodhead, J.D., Hellstrom, J., Hergt, J.M., Greig, A. and Maas, R. (2007) Isotopic and Elemental Imaging of Geological Materials by Laser Ablation Inductively Coupled Plasma-Mass Spectrometry. *Geostand. Geoanal. Res.* 31, 331-343.

Yoshimura, T., Suzuki, A. and Iwasaki, N. (2015) Ba, B, and U element partitioning in magnesian calcite skeletons of Octocorallia corals. *Biogeosci. Discuss.* 12, 413-444.

Zanchetta, G., Drysdale, R.N., Hellstrom, J.C., Fallick, A.E., Isola, I., Gagan, M.K. and Pareschi, M.T. (2007) Enhanced rainfall in the Western Mediterranean during deposition of sapropel S1: stalagmite evidence from Corchia cave (Central Italy). *Quatern. Sci. Rev.* 26, 279-286.

Zhou, H., Chi, B., Lawrence, M., Zhao, J., Yan, J., Greig, A. and Feng, Y. (2008) High-resolution and precisely dated record of weathering and hydrological dynamics recorded by manganese and rare-earth elements in a stalagmite from Central China. *Quat. Res.* 69, 438-446.

Appendix 1: Supplementary Information for Drysdale et al.

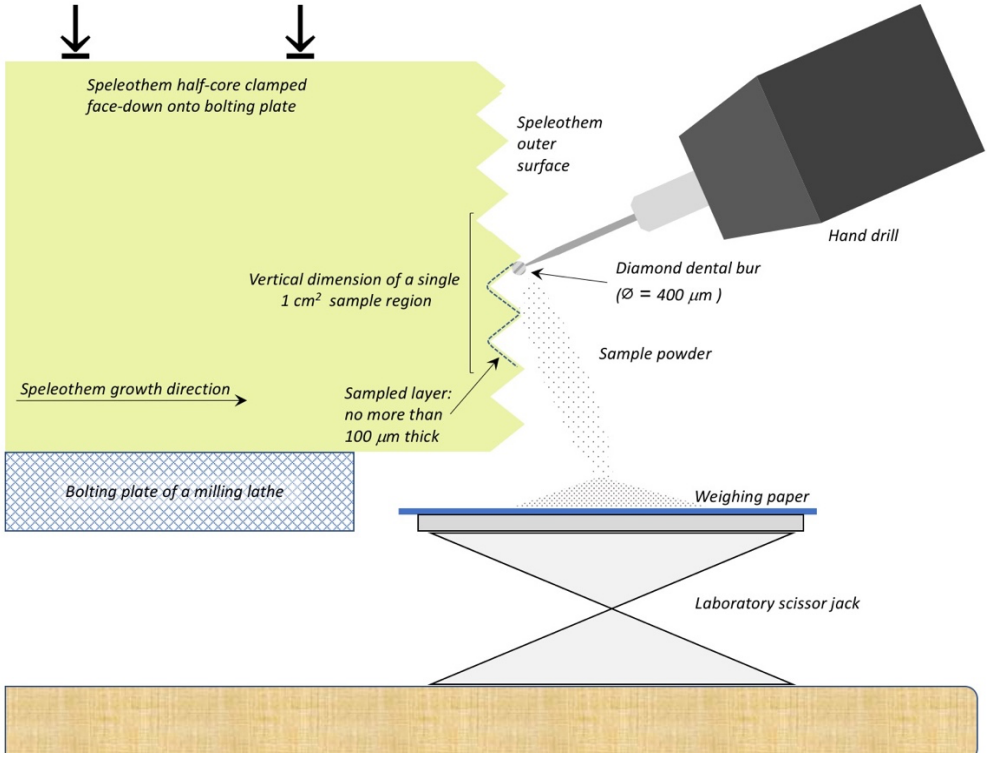

Figure A1: Schematic diagram showing the set-up for sampling of the outer surface of CD3-12. The crystal chevrons at the active growth surface (right side) are exaggerated to better illustrate the process. On each ca. 1 cm^2 area, the milling bit of the hand drill was passed once over each area of exposed crystal. A magnification lamp was used to guide the motion of the hand drill.

Table A1: Selected geochemical data from the 'Grezzoni' dolomite unit in the vicinity of Monte Corchia.

	CO_2 *Wt %*	*CaO* *Wt %*	*MgO* *wt%*	*Sr* *ppm*	*Ba* *ppm*	*Mg/Ca* *(mol/mol)*	*Sr/Ca* *(mmol/mol)*	*Ba/Ca* *(mmol/mol)*
Cortecci et al (1999)								
Gr31	46.7	29.9	22.4	95		1.04	0.203	
Gr32	46.2	29.4	21.6	108		1.02	0.235	
Gr33	46.9	29.1	22.6	74		1.08	0.163	
Azzaro et al. (1987)								
TC3	43.0	28.3	20.7	190	50	1.02	0.430	0.072
TC4	47.1	31.2	21.4	75	50	0.95	0.154	0.065
TC5	46.1	30.0	21.7	152	50	1.01	0.325	0.068
TC7	46.7	30.5	21.7	140	49	0.99	0.294	0.066
TC8	46.5	30.4	22.3			1.02		
TC9	46.4	30.0	22.0	120	51	1.02	0.256	0.069
TC10	46.8	30.2	22.1	152	50	1.02	0.322	0.068
TC12	45.1	29.3	21.6			1.03		
TC13	47.3	31.0	22.1	120	48	0.99	0.248	0.063
TC14	47.3	30.0	22.0	120	48	1.02	0.256	0.065
TC15	46.5	30.5	21.9	154	50	1.00	0.323	0.067
TC16	46.6	30.5	22.2	160	50	1.01	0.336	0.067
TC17	47.3	31.0	21.4	134	46	0.96	0.277	0.061
TC18	46.1	30.2	21.8	136	48	1.00	0.288	0.065
TC19	46.6	31.0	21.4	152	51	0.96	0.314	0.067
TC20	47.2	31.0	22.0	160	44	0.99	0.331	0.058
TC23	45.8	31.9	20.0	200	50	0.87	0.401	0.064
Average	**46.4**	**30.3**	**21.7**	**135.7**	**49.0**	**1.000**	**0.286**	**0.066**
1 s.d.	**1.0**	**0.8**	**0.6**	**34.4**	**1.9**	**0.042**	**0.072**	**0.003**

CD3-12 chronology

A chronology for the upper section of core CD3-12 was indirectly derived using age data from Corchia Cave stalagmite CC26 (Bajo et al. 2016) via a synchronisation process involving two other core samples from CD3 that were drilled in 2007. These have been analysed for various climate proxies since this time, with the relevant data for this study as follows:

- CD3-1: Mg and stable C and O isotopes;
- CD3-2: U-Th dating and Mg;
- CD3-12: Mg.

The cores can be synchronised to one another using their Mg profiles. The procedure is described below.

Stable isotope samples ($\delta^{18}O$ and $\delta^{13}C$) spanning the upper 6.1 mm of CD3-1 were milled at 100-μm increments using a New Wave Micromill. They were analysed by CF-IRMS at the Institut für Geologie und Paläontologie at the Universität Innsbruck using a ThermoFinnigan Delta^{plus}XL. The method is described by Spötl and Vennemann (2003). The long-term analytical uncertainty for oxygen and carbon are 0.08‰ and 0.06‰ respectively (Spötl, 2011). A Mg series was generated by LA-ICP-MS using a Varian 810 quadrupole mass spectrometer coupled to a HelEx laser system (described in Woodhead et al. 2007). To remove surface contaminants, the CD3-1 section was cleaned by two 15-minute rounds of ultrasonication in double-dionised water then twice pre-ablated. (NB: an identical procedure was used on the two other sections reported below.) The final data was collected using a 120 μm spot, a scan speed of 22 μm per second and a laser pulse rate of 5 Hz.

Powdered samples spaced 1 mm apart were drilled from the upper 7 mm of core CD3-2 using a 1-mm-diameter bit. The powders were prepared for U-Th measurement on a Nu Instruments Plasma multi-collector ICP-MS at the School of Earth Sciences, The University of Melbourne, using the methods outlined in Hellstrom (2003) and Drysdale et al. (2012). The U-Th age results are shown in **Table A2**. An age model was produced by linear interpolation (**Figure A2**). A Mg series from CD3-2 was generated immediately adjacent to the drill-hole path by LA-ICP-MS using an Agilent 7700x quadrupole instrument coupled to the same laser system described above. The sample was cleaned as described above, and the data collected using a 19-μm spot size, a scan speed of 5 μm per second and a pulse rate of 10 Hz.

The chronology from CD3-2 was placed onto the depth profile of CD3-1 by synchronising the Mg profiles of the two core sections using *AnalySeries* (Paillard et al. 1996) (**Figure A3**). The resulting stable isotope time series are shown in **Figure A4**. To evaluate the accuracy of the CD3 chronology we compared the CD3-1 $\delta^{18}O$ and $\delta^{13}C$ time series with those from stalagmite CC26 (Bajo et al. 2016), collected adjacent to the cave pool (**Figure A5a,b**). The comparison reveals that both CD3-1 series are shifted to older ages compared to the corresponding series in CC26. We tuned the CD3-1 profiles to CC26, which allows us to provide a crude estimate of the age offset between the CD3-1 and CC26 age models (**Figure A5c**). The average offset is about 2000 years. However, given the large U-Th age sampling error and the linear interpolation of the age model, these offset estimates themselves will have large uncertainties.

Table A2: Uranium-thorium age results from the upper ~7 mm of CD3-2.

Sample ID	CD3 depth (mm)	Depth error (±mm)	$^{230}Th/^{238}U$ measured activity	$^{230}Th/^{238}U$ 2SE	$^{234}U/^{238}U$ measured activity	$^{234}U/^{238}U$ 2SE	Uncorr. age (ka)	95% age error	$^{232}Th/^{238}U$ measured activity	$^{232}Th/^{238}U$ 2SE	$^{230}Th/^{232}Th$ activity	Corr. age (ka)	95% age error	$^{234}U/^{238}U$ initial	$^{234}U/^{238}U$ initial 95% error
CD3-2000	0.50	0.50	0.0196	0.0009	0.6584	0.0009	3.304	0.155	0.000156	0.000002	125.6	**3.27**	**0.16**	0.6552	0.0009
CD3-2001	1.50	0.75	0.0318	0.0013	0.6653	0.0061	5.363	0.231	0.000181	0.000003	175.7	**5.32**	**0.24**	0.6602	0.0062
CD3-2002	2.50	0.75	0.0443	0.0010	0.6656	0.0027	7.552	0.181	0.000118	0.000007	374.3	**7.52**	**0.18**	0.6584	0.0028
CD3-2003	3.50	0.75	0.0769	0.0016	0.6667	0.0033	13.501	0.311	0.000098	0.000003	782.3	**13.48**	**0.31**	0.6538	0.0035
CD3-2004	4.50	0.75	0.0825	0.0013	0.6760	0.0037	14.340	0.260	0.000376	0.000004	219.5	**14.25**	**0.28**	0.6627	0.0039
CD3-2005	5.50	0.75	0.1415	0.0015	0.6821	0.0022	25.841	0.331	0.000378	0.000007	374.6	**25.74**	**0.34**	0.6581	0.0025
CD3-2006	6.50	0.75	0.1658	0.0016	0.6924	0.0025	30.508	0.373	0.001087	0.000006	152.5	**30.24**	**0.46**	0.6650	0.0029

Notes

1. All ratios are activity ratios, determined following Hellstrom (2003).
2. Ages are in kyr before time of analysis, calculated using the decay constants of Cheng et al. (2013).
3. Corrected ages are calculated using equation 1 of Hellstrom (2006) and an assumed initial ($^{230}Th/^{232}Th$) of 1.5 ± 1.5.
4. Initial ($^{234}U/^{238}U$) is calculated using the corrected age.
5. Uncertainties are two standard error (2SE) for measured ratios, and 95% confidence for (Monte-Carlo) calculated ages.

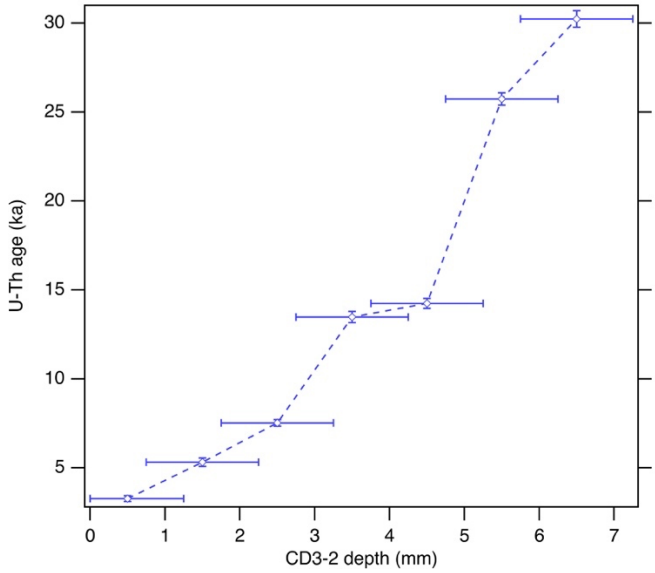

Figure A2: Depth-age plot and age model based on linear interpolation of the seven U-Th ages shown in Table A2.

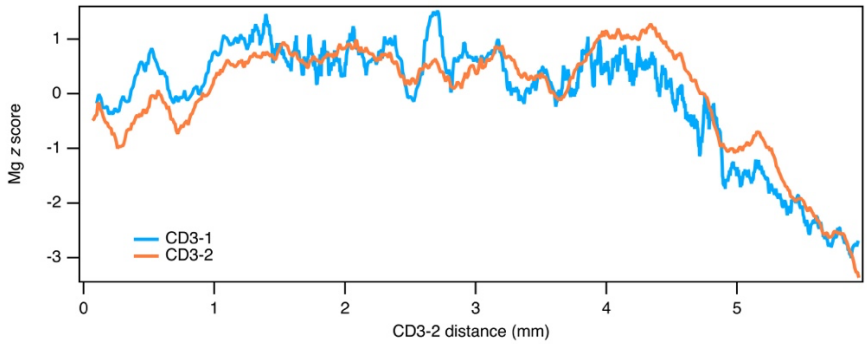

Figure A3: Mg profiles from CD3-1 (blue) and CD3-2 (orange) synchronized to the CD3-2 depth scale using *Analyseries*. Both series have been smoothed (15-pt running mean) to remove high-frequency variability.

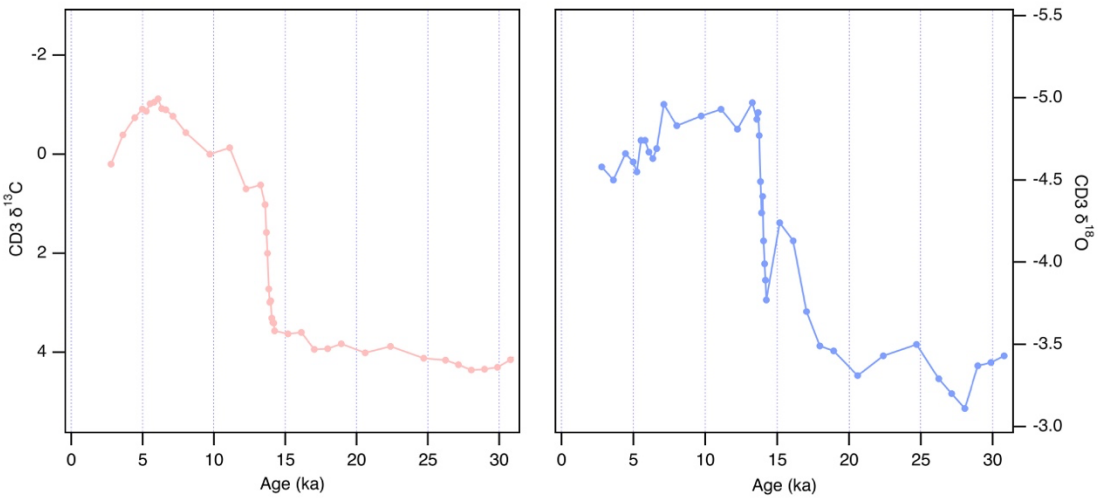

Figure A4: Stable isotope time-series from CD3-1 based on U-Th ages from CD3-2. The age model was interpolated from CD3-2 by synchronizing the Mg profiles from each core (Figure A3).

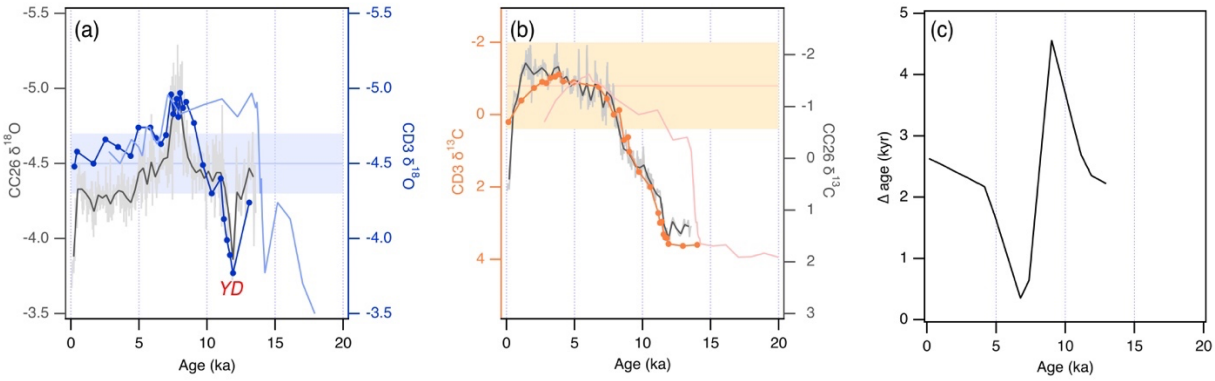

Figure A5: **(a-b)** Comparison between the CD3-1 and CC26 stable isotope time series. The raw original CC26 data are shown in light grey. To facilitate the comparison, the CC26 data were decimated to approximately the same resolution as CD3-1 (dark grey). The CD3-1 time series based on the CD3-2 age model (Figure A2) is shown in pale blue ($\delta^{18}O$) and pale orange ($\delta^{13}C$). The result of tuning the CD3-1 $\delta^{18}O$ and $\delta^{13}C$ series to CC26 is shown in the dark blue ($\delta^{18}O$) and dark orange ($\delta^{13}C$) series with solid circles. The coloured horizontal bands show the mean and 95% uncertainties of modern $\delta^{18}O$ and $\delta^{13}C$ values collected from four stalagmites. 'YD' denotes the position of the Younger Dryas stadial in the $\delta^{18}O$. **(c)** The age offset for the CD3-1 series derived from subtracting the CC26 age from the CD3-1 age.

Note that the trend towards higher stable isotope values over the last few centuries in CC26 is likely a kinetically induced response (evaporation) to a decline in drip rate, which culminated in cessation of this stalagmite's growth within the last century. This is reinforced by the presence of aragonite in the upper millimetre and the decrease in growth rates (discussed in Bajo et al. 2016) and evident in the age model of Figure 2 of that paper. This explains the anomaly between $\delta^{18}O$ and $\delta^{13}C$ isotope values at the top of CD3 and CC26. Isotopic measurements made on calcite from the tips of four stalagmites (coloured horizontal bands in Figure A5) located within a 20-metre radius of CD3 give $\delta^{18}O$ and $\delta^{13}C$ compositions consistent with the top of CD3.

LA-ICP-MS Mg analysis was carried out on the upper section of CD3-12 using the following settings: a square spot size of 25 µm, a pulse rate of 5 Hz and a scan speed of 1 mm per minute. The Mg profile can be synchronised to that of Mg of CD3-2 (Figure A6a), allowing the CC26-corrected age model to be mapped to CD3-12.

The end of the Younger Dryas stadial, which is evident in both the CD3-1 and CC26 $\delta^{18}O$ series (Figure A5), marks the start of the Holocene. The corresponding depth position of the YD-Holocene boundary (~11.65 ka) in CD3-12 from the age model corresponds to 3.96 mm (Figure A6b), giving a mean Holocene growth rate for CD3-12 of 0.34 µm per year.

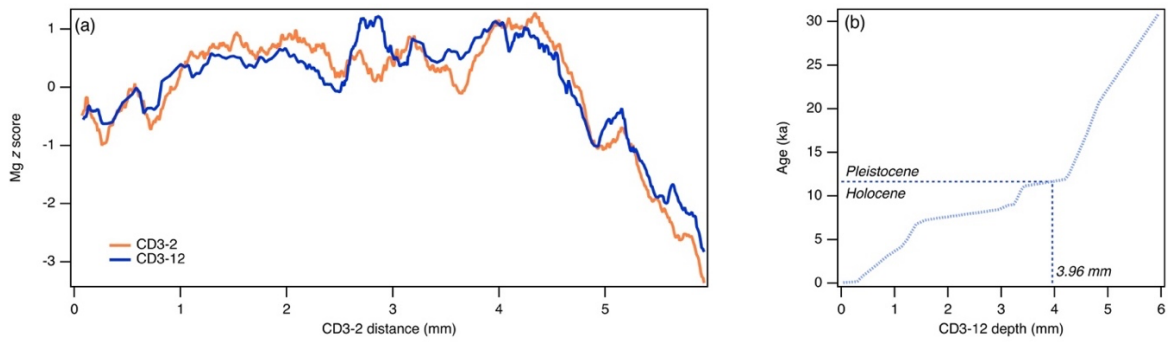

Figure A6: (a) Synchronisation of the CD3-2 and CD3-12 Mg series. This enables the corrected age model for CD3-2 (based on Figure A5) to be applied to CD3-12. **(b)** CC26-corrected CD3-12 age model showing the depth position of the Pleistocene-Holocene transition (3.96 mm).

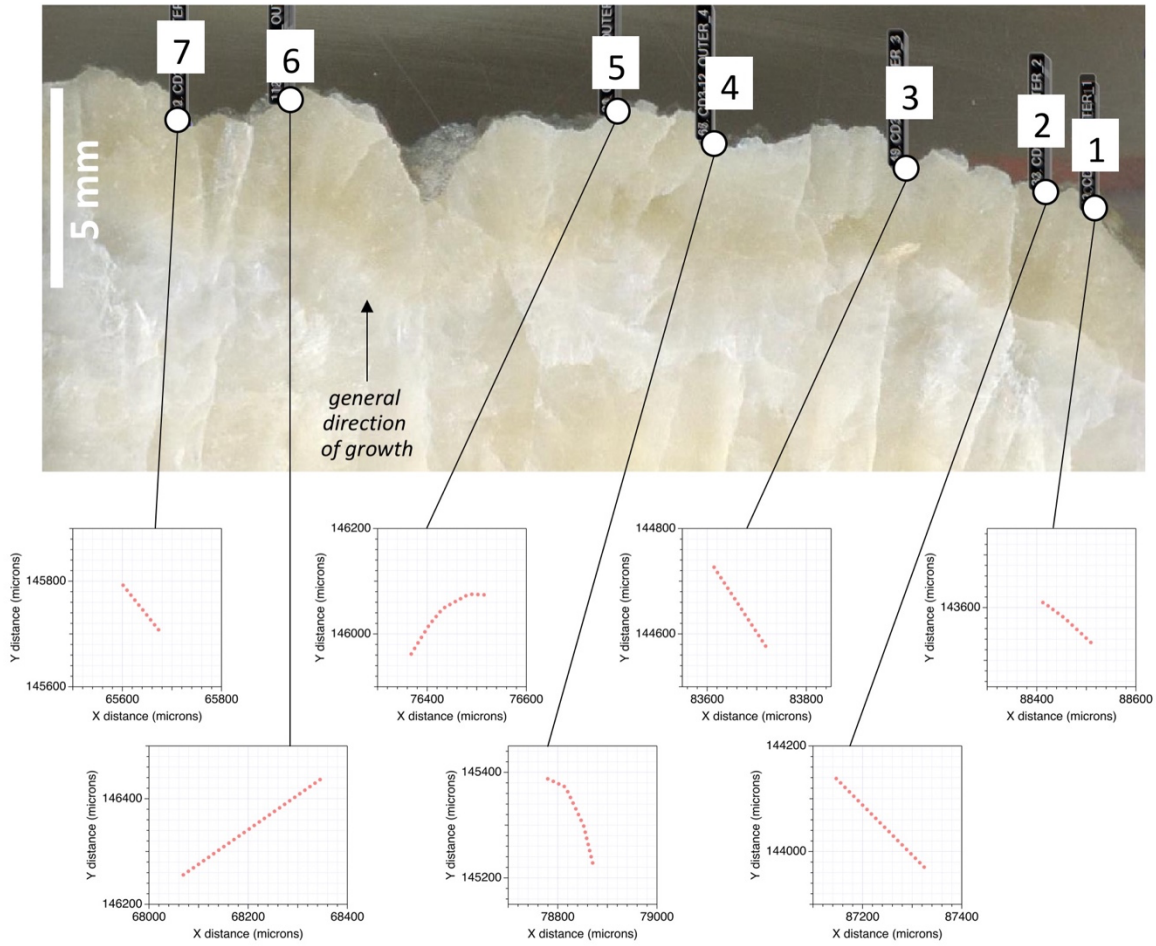

Figure A7: Polished-section image of the upper surface of CD3-12 showing the position of the high-resolution LA-ICP-MS traverses. The image was captured whilst the section was positioned in the laser-ablation cell, with the laser-beam position orthogonal to the image plane. Each traverse, the position of which is indicated by white circles, followed the outermost edge of the calcite, i.e. the actively growing outer surface. Enlargements of each traverse are plotted on the actual coordinate system of the *Geostar* software. The orientation of each traverse follows exactly that of the relevant crystal face.

Table A3: Results from the measurement of additional hydrochemical parameters for Laghetto Basso.

Date	*Temp. (°C)*	*pH*	*Na (mg L^{-1})*	*Cl (mg L^{-1})*	*SO_4 (mg L^{-1})*	*PCO_2 (atm)*	*SI_{cal}*	*% charge balance*
22/05/09	8.0	8.33	4.1	5.8	30.4	0.00051	0.42	0.8
17/06/09	7.3	8.35	4.1	5.6	30.6	0.00050	0.45	0.0
28/07/09	8.1	8.04	3.9	5.4	30.8	0.00102	0.15	1.4
28/08/09	8.0	8.39	3.9	5.5	30.3	0.00045	0.49	0.0
02/10/09	8.1	8.26	3.9	5.3	29.3	0.00060	0.36	-0.4
14/11/09	7.9	8.21	3.9	5.5	31.2	0.00064	0.26	-2.2
14/12/09	8.0	8.29	3.8	4.5	31.9	0.00056	0.37	-0.3
24/02/10	8.0	8.22	3.7	4.4	31.0	0.00072	0.35	-0.8
27/03/10	8.0	8.13	3.8	6.6	30.8	0.00082	0.23	1.0
19/04/10	7.9	8.35	3.9	5.3	29.4	0.00049	0.43	0.0
31/05/10	7.8	8.27	4.0	5.4	29.9	0.00061	0.37	-1.2
29/06/10	7.8	8.28	2.1	3.4	30.6	0.00056	0.37	1.8
05/08/10	7.9	8.27	3.9	5.7	30.5	0.00057	0.34	1.5
01/09/10	7.9	8.25	3.9	5.4	33.1	0.00060	0.32	1.0
30/09/10	7.9	8.26	3.7	5.1	37.7	0.00057	0.31	-0.2
29/10/10	7.9	8.18	4.4	5.4	31.5	0.00070	0.23	0.6
25/11/10	7.9	8.12	3.6	5.7	34.7	0.00086	0.23	-1.3
29/12/10	7.9	8.12	3.9	5.5	32.7	0.00082	0.21	0.8
03/02/11	7.5	8.15	3.7	5.6	31.3	0.00075	0.21	0.8
10/03/11	8.0	8.19	3.6	5.1	30.6	0.00072	0.29	-0.7
05/04/11	7.8	8.22	3.8	5.6	28.5	0.00066	0.30	1.2
11/05/11	7.7	8.21	3.7	5.6	30.9	0.00066	0.28	2.0
24/06/11	7.6	8.21	4.1	5.8	31.6	0.00070	0.31	-0.4
11/07/11	7.8	8.08	4.1	5.6	31.5	0.00090	0.16	1.8
09/08/11	7.4	8.11	3.9	5.4	31.0	0.00082	0.16	0.2
06/10/11	7.9	8.19	3.9	5.5	31.9	0.00071	0.28	2.4
07/11/11	8.4	8.08	3.9	5.3	34.2	0.00088	0.15	1.6
23/03/12	8.1	7.93	3.9	5.5	31.0	0.00130	0.06	1.9
Mean	**7.9**	**8.20**	**3.8**	**5.3**	**31.7**	**0.00070**	**0.27**	
2σ	**0.2**	**0.10**	**0.8**	**1.2**	**3.9**	**0.00018**	**0.18**	
% CV (2σ)	**5.2**	**2.3**	**22.1**	**23.0**	**12.3**	**47.5**	**66.2**	
n	**28**	**28**	**28**	**28**	**28**	**28**	**28**	

Table A4: LA-ICP-MS data for Mg, Sr, Ba and U (all in ppm) from all spots (n = 120).

Traverse	^{24}Mg	^{88}Sr	^{138}Ba	^{238}U	*Traverse*	^{24}Mg	^{88}Sr	^{138}Ba	^{238}U
1	10790	70.1	22.9	1.23	4	11850	75.2	26.1	1.27
1	10290	66.9	24.3	1.44	4	11540	74.5	25.3	1.28
1	10140	68.7	24.3	1.40	4	12270	73.4	24.9	1.30
1	10610	74.0	24.7	1.30	4	11010	72.9	26.7	1.38
1	11560	79.3	27.7	0.78	4	11040	71.3	25.8	1.51
1	11360	72.4	25.4	1.30	5	11650	78.2	38.7	1.41
1	10820	67.5	24.2	1.35	5	12360	71.1	23.6	1.29
1	11500	72.3	24.3	1.18	5	12030	75.9	27.5	1.22
1	11410	72.0	24.9	1.41	5	11210	68.1	24.5	1.35
1	11500	70.9	24.5	1.19	5	11410	71.8	24.4	1.39
1	10930	64.3	21.0	1.42	5	11310	71.1	26.9	1.22
2	10740	68.0	23.5	1.11	5	11220	74.1	27.8	1.61
2	11290	70.3	23.1	0.93	5	11560	73.2	26.7	1.29
2	10860	77.2	24.9	0.86	5	11200	68.8	25.1	1.51
2	11110	75.2	26.3	1.30	5	10790	75.4	26.9	1.79
2	10660	68.8	23.9	1.46	5	10930	71.5	25.3	1.46
2	11220	76.0	26.1	1.27	5	11440	71.2	27.2	1.36
2	11480	76.8	25.8	0.75	5	11730	75.0	27.2	1.59
2	10900	71.0	24.1	1.56	5	11400	73.8	25.3	1.46
2	11690	72.5	25.6	1.20	5	11430	70.4	24.9	1.43
2	11590	71.0	23.6	1.00	5	11150	77.2	27.3	1.47
2	11360	70.2	22.4	1.06	5	10920	67.6	21.5	1.41
2	11780	68.0	23.6	0.77	6	12900	88.7	34.6	0.13
2	11940	69.8	21.7	0.97	6	11290	79.8	26.0	0.36
2	11710	68.4	21.3	0.96	6	10430	71.0	21.4	0.99
2	11750	73.2	23.0	0.73	6	10960	63.6	19.8	1.37
2	11830	73.3	24.3	0.89	6	12020	78.7	26.1	0.56
2	11250	78.0	28.0	0.87	6	12130	80.0	24.0	0.36
2	12020	74.7	24.4	0.63	6	12620	82.1	34.3	0.23
2	11080	70.2	26.3	1.40	6	11720	81.6	27.1	0.27
2	11440	74.2	23.9	0.87	6	10850	78.5	25.3	0.69
2	11320	72.8	22.2	0.83	6	11710	77.7	25.7	0.76
3	11060	71.6	24.5	1.34	6	12090	74.4	24.0	0.73
3	11780	73.1	25.6	1.24	6	12090	74.2	23.6	0.65
3	11120	72.2	25.2	1.42	6	11420	73.1	26.2	0.97
3	11700	73.3	25.0	1.08	6	11940	75.8	26.5	1.06
3	11720	70.0	23.8	1.46	6	11550	77.5	26.2	0.76
3	11200	71.1	24.0	1.41	6	11460	76.6	28.8	1.25
3	11580	71.5	24.0	1.15	6	11260	74.8	26.1	1.20
3	11620	70.1	22.5	1.27	6	12280	71.6	22.9	0.71
3	11210	69.5	23.9	1.45	6	12040	72.5	21.9	0.64
3	11430	71.0	25.0	1.45	6	11760	72.4	24.5	0.78
3	11490	72.5	25.9	1.42	6	11650	74.9	26.2	0.74
3	11010	72.2	23.1	1.41	6	11250	73.1	28.1	1.26
3	11160	72.7	23.8	1.42	6	11530	76.7	27.0	1.11
3	11270	71.8	25.3	1.59	6	11420	73.4	24.4	1.31
3	11240	74.5	25.2	1.60	6	11180	73.3	26.4	1.08
3	11490	75.7	26.5	1.35	6	11010	71.4	24.5	1.37
4	11320	72.4	25.0	1.39	6	11260	67.0	23.0	1.18
4	11350	74.5	27.4	1.36	6	11180	69.9	22.4	1.13
4	11350	75.4	27.2	1.40	7	11040	66.1	21.4	1.31
4	11600	71.7	26.1	1.25	7	10780	66.8	23.3	1.36
4	11580	73.8	25.5	1.48	7	10830	69.3	23.7	1.57
4	11480	75.8	26.5	1.39	7	11020	65.3	23.3	1.28
4	11060	69.6	25.3	1.46	7	11590	69.9	22.4	1.10
4	11350	74.6	25.5	1.42	7	11080	64.9	23.7	1.39
4	10800	69.4	23.8	1.44	7	11650	74.0	25.3	1.34
4	11390	72.8	26.6	1.43	7	11090	67.6	24.5	1.35
4	11090	71.7	26.0	1.58	7	10830	70.7	24.9	1.44
4	11410	68.7	24.0	1.53	7	11060	68.4	22.5	1.07

Additional references

Cheng, H, Lawrence Edwards, R, Shen, C, Polyak, V, Asmerom, Y, Woodhead, J, Hellstrom, J, Wang, Y, Kong, X & Spotl, C. (2013) Improvements in ^{230}Th dating, ^{230}Th and ^{234}U half-life values, and U-Th isotopic measurements by multi-collector inductively coupled plasma mass spectrometry. *Earth and Planetary Science Letters* 371-372, 82–91, doi:10.1016/j.epsl.2013.04.006.

Hellstrom, J.C. (2003) Rapid and accurate U/Th dating using parallel ion-counting multi-collector ICP-MS. *Journal of Analytical Atomic Spectrometry* 18, 1346–1351, doi:10.1039/b308781f.

Paton, C., Hellstrom, J., Paul, B., Woodhead, J., Hergt, J., 2011. Iolite: freeware for the visualisation and processing of mass spectrometer data. *Journal of Analytical Atomic Spectrometry* 26, 2508-2518.

Paillard, D, Labeyrie, L & Yiou, P. (1996) AnalySeries 1.0: a Macintosh software for the analysis of geophysical time-series', *Eos*, vol. 77, p. 379.

Spötl, C. & Vennemann, T. W. (2003) Continuous-flow isotope ratio mass spectrometric analysis of carbonate minerals. *Rapid Commun. Mass Spectrom.* 17, 1004–1006.

Spötl, C. (2011) Long-term performance of the Gasbench isotope ratio mass spectrometry system for the stable isotope analysis of carbonate microsamples. *Rapid Commun. Mass Spectrom.* 25, 1683-1685.

Woodhead, J., Hellstrom, J., Hergt, J.M., Greig, A., Maas, R. (2007) Isotopic and elemental imaging of geological materials by laser ablation inductively coupled plasma-mass spectrometry. *Geostandards and Geoanalytical Research* 31, 331-343.